HHS Public Access

Author manuscript

Biophys Chem. Author manuscript; available in PMC 2018 May 01.

Published in final edited form as:

Biophys Chem. 2017 May ; 224: 1–19. doi:10.1016/j.bpc.2017.02.006.

Calcium Triggers Reversal of Calmodulin on Nested Anti-Parallel Sites in the IQ Motif of the Neuronal Voltage-Dependent Sodium Channel $Na_V1.2$

Liam Hovey[1,+], **C. Andrew Fowler**[2,+], **Ryan Mahling**[1], **Zesen Lin**[1], **Mark Stephen Miller**[1], **Dagan C. Marx**[1], **Jesse B. Yoder**[1], **Elaine H. Kim**[1], **Kristin M. Tefft**[1], **Brett C. Waite**[1], **Michael D. Feldkamp**[1], **Liping Yu**[2], and **Madeline A. Shea**[1,*]

[1]Department of Biochemistry, Roy J. and Lucille A. Carver College of Medicine, University of Iowa, Iowa City, Iowa 52242-1109

[2]NMR Facility, Roy J. and Lucille A. Carver College of Medicine, University of Iowa, Iowa City, Iowa 52242-1109

Abstract

Several members of the voltage-gated sodium channel family are regulated by calmodulin (CaM) and ionic calcium. The neuronal voltage-gated sodium channel $Na_V1.2$ contains binding sites for both apo (calcium-depleted) and calcium-saturated CaM. We have determined equilibrium dissociation constants for rat $Na_V1.2$ IQ motif [IQRAYRRYLLK] binding to apo CaM (~3 nM) and $(Ca^{2+})_4$-CaM (~85 nM), showing that apo CaM binding is favored by 30-fold. For both apo and $(Ca^{2+})_4$-CaM, NMR demonstrated that $Na_V1.2$ IQ motif peptide ($Na_V1.2_{IQp}$) exclusively made contacts with C-domain residues of CaM (CaM_C). To understand how calcium triggers conformational change at the CaM-IQ interface, we determined a solution structure (2M5E.pdb) of $(Ca^{2+})_2$-CaM_C bound to $Na_V1.2_{IQp}$. The polarity of $(Ca^{2+})_2$-CaM_C relative to the IQ motif was opposite to that seen in apo CaM_C-$Na_v1.2_{IQp}$ (2KXW), revealing that CaM_C recognizes nested, anti-parallel sites in $Na_v1.2_{IQp}$. Reversal of CaM may require transient release from the IQ motif during calcium binding, and facilitate a re-orientation of CaM_N allowing interactions with non-IQ $Na_V1.2$ residues or auxiliary regulatory proteins interacting in the vicinity of the IQ motif.

Graphical abstract

*Corresponding author. Telephone: (319) 335-7885. FAX: (319) 335-9570, madeline-shea@uiowa.edu.
+These authors contributed equally to this work.

Accession Numbers

The coordinates for the average minimized structure and 20 lowest energy models were deposited with the PDB code of 2M5E; there were preliminary conference reports of this structure.[142, 143] NMR assignment data (accession number 19050) were deposited with the BioMagResBank (BMRB http://www.bmrb.wisc.edu). Assignments are also contained in Supplemental Tables S2 and S3.

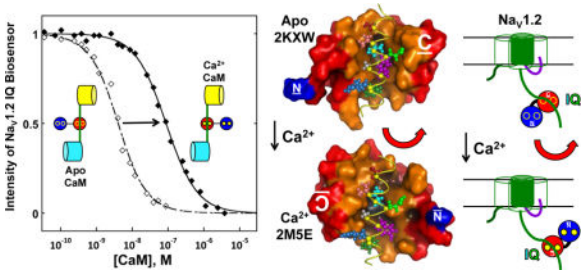

Keywords

Molecular Recognition; Allostery; NMR; Titration; Binding; Linkage; Biosensor; Thermodynamics; Free Energy; Sodium Channels; FRET

1. Introduction

The human voltage-dependent sodium channel family (Na_V) is responsible for the generation and propagation of action potentials.[1, 2] Na_V channelopathies include epilepsy [3], “Long QT” syndrome [4], familial autism [5] and pain insensitivity.[6] Na_V channels are believed to undergo calcium-dependent regulation[7] mediated by calmodulin (CaM), an essential intracellular calcium sensor.[8] However, the mechanisms of calcium-induced regulation remain poorly understood, and may vary among Na_V subtypes.[9]

1.1 Universal Design for Apo CaM binding to Na_V IQ motifs

The architecture of the $Na_V1.2$ pore-forming α-subunit (2005 a.a.) is shown in Fig. 1A. It has 4 multi-helical transmembrane domains (green cylinders) that form the ion-conducting pore and contain voltage-sensing domains; they are connected by intracellular linkers.[10] The $Na_V1.2$ C-terminal domain (CTD) contains a 4-helix bundle (EF-like or EFL domain) that preferentially binds FGF12[11] but also binds other members of the FGF homology factor (FHF) family. A solution structure (2KAV[12]) of a fragment of $Na_V1.2$ that includes EFL (Fig. 1B) shows that the next (fifth) helix is connected to EFL by a flexible linker, allowing it to adopt many orientations relative to the 4-helix bundle. A schematic diagram of a fragment of the $Na_V1.2$ CTD sequence below 2KAV shows the relative length and position of the helices within 2KAV that precede the helix containing the IQ motif (IQxxx[R,K]Gxxx[R,K][13]) that binds CaM tightly [14–16]. The IQ motif is necessary for several members of the human Na_V family to maintain a closed, inactivated state.[17, 18]

Five high-resolution structures of apo (calcium-depleted) CaM bound to Na_V IQ motifs are available. In all of these structures, CaM_C adopts the semi-open tertiary structure also observed in complexes of apo CaM_C bound to myosin V [19] and the SK Channel[20]. A crystal structure of apo CaM bound to a CTD fragment of cardiac $Na_V1.5$ (4DCK, Fig. 1C) shows the C-domain of CaM (CaM_C) binds to the IQ motif, while the N-domain (CaM_N) makes few contacts with any part of the CTD. An overlay of this complex with apo CaM bound to the IQ motifs from $Na_V1.2$[16], $Na_V1.5$[21–23] and $Na_V1.6$[24] (Fig. 1D) illustrates that the position of apo CaM_N is highly variable relative to CaMC.

The five structures are shown individually in Fig. 1E (note that CaM_N is not shown for $Na_V1.2$ (2KXW) because the structure included only CaM_C). The solution structure of apo CaM bound to $Na_V1.5$ (2L53) shows the ensemble of models included in the PDB deposit, with CaM_N. having no preferred position relative to CaM_C. In two crystallographic structures (4DCK and 4OVN) of CaM bound to a fragment of $Na_V1.5$, there are distinct differences in the observed position of CaM_N, perhaps attributable to differences in crystal contacts, solution conditions, or an additional auxiliary protein (FGF13U/FHF2) bound to the $Na_V1.5$ fragment in 4DCK (not shown). Residues in $Na_V1.5$ and $Na_V1.6$ that make multiple contacts with CaM (spheres, Fig. 1D) include residues in positions analogous to $Na_V1.2$ Y_{1916} and Y_{1919} which are highly conserved within $Na_V1.2$ sequences.

Magnesium was resolved in the calcium-binding sites of two of the structures of apo CaM bound to $Na_V1.5$ (Fig. 1E). In 4OVN, Mg^{2+} was observed in all 4 of the calcium-binding sites in CaM, whereas, in 4DCK, Mg^{2+} was seen only in CaM_C sites III and IV (assignment of residues in CaM_N sites I and II was not complete in 4DCK). Magnesium and calcium have different hydration shells, and chelation of magnesium is accomplished with a different geometric signature in the subset of residues required for pentagonal, bipyramidal chelation characteristic of calcium binding to EF-hand loops ([25] illustrated in Supplemental Figure S1A. In the crystallographic structure (3WFN) of apo CaM bound to $Na_V1.6$ IQp, no metal ions were included in the deposited structure.

For $Na_V1.2$, $Na_V1.5$ and $Na_V1.6$, WebLogos [26] in Fig. 1F illustrate the highly similar sequences preceding and comprising their IQ motifs [IQRAϕRRϕxxK1 (alignments are provided in Supplemental Table S1). All are basic, amphipathic alpha helices (BAA motifs) characteristic of CaM binding domains. For example, the rat NaV1.2 IQ peptide has a calculated pl of 10.75, and a predicted net charge of +8 at pH 7. Consistent with their similarity in sequence, the available high-resolution structures (Fig. 1E) show that regardless of Na_V isoform or structural method (NMR, XRD) used for determination, the “IQ” residues are in identical positions. The I (cyan) of $Na_V1.2$ and $Na_V1.5$, and L (cyan) in the equivalent position of $Na_V1.6$ are buried in the semi-open cleft of CaM_C. The fully conserved Q (green) residue of each IQ motif is oriented toward the F-G linker of CaM, forming a network of hydrogen bonds.

1.2 What Does Calcium Binding Do to CaM-Na_V Interactions?

While these analyses illustrate the conformation of CaM associated with the Na_V IQ motif under low “resting calcium” conditions, they do not explain the role of calcium in modulating CaM-Na_V interactions. Early studies identifying the preferred sites for CaM binding to the CTD of $Na_V1.2$ showed that sites for apo CaM and $(Ca^{2+})_4$-CaM were overlapping but slightly different [14], suggesting that $(Ca^{2+})_4$-CaM might slide towards the C-terminus of $Na_V1.2$ upon binding calcium.

Calcium binding is known to trigger large changes in interhelical angles within both domains of CaM. In hundreds of high-resolution structures of CaM – whether free or bound to a peptide derived from a target protein–calcium-free domains of CaM are always observed to adopt a closed or semi-open conformation. The open tertiary structure is only observed when calcium occupies the loops in the helix-loop-helix motifs. This is illustrated

in Fig. 2A, showing apo CaM_C alone (1CFC) and bound to a myosin V peptide (2IX7), and calcium-saturated CaM_C alone (1CLL) and bound to a CaMKII peptide (1CDM). The alignment by residues in helix G highlights the opening of the CaMC cleft in response to calcium binding; helices E and F are depicted in black. This grid also demonstrates that the orientation of the CaMBD (CaM-binding domain) peptide from myosin V bound to apo CaM is opposite to that of the CaMKII peptide bound to calcium-saturated CaMC. This plasticity in the calcium-dependent interactions of CaM with its targets is a hallmark feature of its role as a hub protein in signaling networks.[27–32]

1.3 Distinct Responses by CaM_C and CaM_N

The linker between CaM_C and CaM_N allows the two domains to adopt many different relative orientations. Full-length $(Ca^{2+})_4$-CaM may be extended as seen in the crystallographic structure in Fig. 2B where the linker is helical, fully separating CaM_N and CaM_C. In contrast, Fig. 2C shows the two domains of $(Ca^{2+})_4$-CaM wrapped around the CaMBD peptide of CaMKII (compact ellipsoidal). However, an overlay (Fig. 2D) of CaMC from Figs. 2B and 2C shows that CaMC adopts an open tertiary conformation in both, and has identical geometry of calcium-chelating residues in the calcium-binding sites, with the bidentate glutamates E104 (site III) and E140 (site IV), each at position 12 of an EF-hand loop (sticks in red or orange), providing two oxygens for holding Ca^{2+} in the respective site. The geometry of the calcium-binding loops and interhelical angles is very different if calcium is not bound.

The domains of CaM function as distinct calcium-sensors and CaM can adopt a half-saturated state in which one domain is apo while both sites in the other domain are occupied by calcium. An example is the structure of half-saturated CaM (having $(Ca^{2+})_2$-CaM_N and apo CaM_C) bound to a fragment of the SK channel (1G4Y). This is compared in Fig. 2E to a structure of apo CaM bound to a peptide from myosin V (2IX7). The apo CaM_C domains are identical in tertiary structure, whereas CaM_N has an open tertiary conformation with calcium bound in 1G4Y. It adopts different positions relative to CaM_C depending on the target peptide bound to CaM. Structures of apo CaM_C bound to IQ motifs of Na_Vs (Fig. 1E) match those observed in 2IX7 and 1G4Y.

Two crystal structures of half-saturated CaM bound to the IQ motif of Na_V CTDs have been published in which calcium occupies sites I and II in CaM_N. For CaM bound to $Na_V1.5$, Fig. 2F shows an overlay of the IQ motif of $Na_V1.5$ bound to apo CaM (4DCK) and calcium-bound CaM (4JQ0). In both structures, CaM_C is in the semi-open tertiary conformation characteristic of apo CaM, and the interface between CaM_C and the $Na_V1.5$ IQ motif is identical. Like the overlay shown in Fig. 2E, CaM_N in 4JQ0 has an open tertiary conformation with calcium bound and adopts positions relative to CaM_C that differ from apo CaM_N in 4DCK. The gray spheres depict the position of magnesium while the red depict calcium. Although both 4JPZ (3.02 A resolution) and 4JQ0 (3.84 A resolution) were deposited in the PDB with calcium having 100% occupancy in sites III and IV of CaM_C, the authors commented that “These conformational differences of the individual CaM lobes in the $Na_V1.2/Ca^{2+}$ structure suggested that the C-lobe was unlikely to be fully occupied,” (p.

4) and that CaM_C "is essentially unoccupied in the $Na_V1.2/Ca^{2+}$ structure" based on anomalous scattering data (p. 6) [33].

1.4 Magnesium and Calcium – Cousins, Not Twins

The conclusion that sites III and IV do not contain calcium is supported by the overlay in Fig. 2G comparing CaM_C in 4DCK and 4JQ0 (both bound to the $Na_V1.5$ IQ motif) and CaM_C in 1G4Y (bound to an SK Channel peptide). All three structures show CaM_C having a semi-open tertiary conformation. The bidentate glutamates (E104 and E140) in sites III and IV (blue 4DCK, cyan 1G4Y) are oriented away from the loop, consistent with the absence of calcium. These orientations are very different from what is observed in calcium-saturated sites shown in Fig. 2D. In 4JQ0, only the alpha carbon of residues E104 and E140 were assigned (the side chain atoms are missing). However the semi-open conformation, and absence of density for chelating carboxyl groups is consistent with the sites being apo.

The tertiary conformation of CaM_C bound to the IQ motif in a fragment of $Na_V1.2$ (4JPZ, Fig. 2H) is identical to that observed in 4JQ0 representing $Na_V1.5$. The conclusion that calcium is absent from CaM_C in 4JPZ is supported by the F_o-F_c electron density maps around the metals in sites III and IV of chains C and I compared to the same sites in a CaM-alone structure (1CLL; Supplemental Figure S1C). Despite the high concentration of calcium in the crystallization buffer (300 mM sodium acetate, 50 mM TRIS, pH 7.5, 2 mM $CaCl_2$,), all of these data suggest that CaM_C maintained the apo state despite calcium binding to CaM_N. Thus, 4JPZ and 4JQ0 represent Na_V CTD fragments bound to a half-saturated complex of CaM like the complex observed in 1G4Y with an SK Channel fragment bound to half-saturated CaM (Fig. 2E).

However, calcium-saturated CaM is known to bind tightly to the IQ motifs in $Na_V1.2$ and $Na_V1.5$.[15, 16, 23, 33–35] A stoichiometric calcium titration of CaM bound to the $Na_V1.2$ IQ motif showed 4 equivalents of calcium were required for saturation ([16], Fig. 7 therein). This raises the question of why sites III and IV in CaM would retain the apo conformation in structures 4JPZ and 4JQ0.

Those structures included a third protein – an intracellular FGF (FHF) isoform that recognizes the EFL domain within Na_V. FGF13U was bound to the $Na_V1.2$ CTD in 4JPZ, and FGF12U was bound to the $Na_V1.5$ CTD in 4JQ0. For $Na_V1.2$ (Fig. 2H), the asymmetric unit includes two heterotrimers (called A and B), and there are many close interactions between them. Close contacts between CaM in one heterotrimer with FGF in the other (i.e., CaM_a-FGF_b and CaM_b-FGF_a) are shown in Fig. 2I, while interactions between residues in the calcium-binding sites of CaM in each heterotrimer are shown in Fig. 2J. These suggest that a network of contacts observed in the crystal structure may provide tertiary constraints that favor retention of the CaM_C-IQ binding interface observed in the absence of calcium.

1.5 Which CaM-Na_V recognition determinants are encoded in the IQ Motif?

Because there is no physiological evidence of which we are aware that CaM interacts with FGF bound to a neighboring channel as seen in the dimer of heterotrimers in 4JPZ, it is expected that these interactions would not occur under native conditions in a neuron. Based on the well characterized effect of calcium triggering opening of hydrophobic clefts in the

domains of CaM [36, 37], we hypothesize that calcium binding to CaM_C bound to the $Na_V1.2$ IQ motif should open the tertiary conformation of the domain to match the cleft observed for structures such as 1CLL or 1CDM, shown in Fig. 2A. Furthermore, based on the original report of CaM binding sites in $Na_V1.2$ [14] and subsequent titrations and thermodynamic linkage studies [7, 15, 16] showing differences in free energies of binding apo and $(Ca^{2+})_4$-CaM, we expect calcium binding to alter the CaM_C-IQ interface seen in apo-CaM-IQ complexes in Fig. 1E.

To compare how apo and $(Ca^{2+})_4$-CaM differ in their recognition of the $Na_V1.2$ IQ motif, we determined calcium-dependent differences in CaM binding to a biosensor comprised of the $Na_V1.2$ IQ motif sequence flanked by YFP and CFP.[38] The exquisite sensitivity of FRET between the autofluorescent proteins allowed direct estimates of equilibrium constants below 100 nM which allows us to distinguish between the very high affinity of both apo and calcium-saturated CaM for the IQ motif.

To understand how calcium alters the interface observed between the $Na_V1.2$ IQ motif and apo CaM_C, we focused exclusively on CaM_C bound to the IQ motif (no EFL) in the absence of auxiliary proteins (no FGF). We eliminated the potential contribution of crystal contacts by determining a high-resolution solution structure (2M5E) of the complex of $(Ca^{2+})_2$-CaM_C bound to $Na_v1.2_{IQp}$. In this structure, $(Ca^{2+})_2$-CaM_C reverses its orientation on the IQ motif relative to the structure (2KXW) of apo CaM_C bound to the same sequence. This pivot in place is a striking structural response to calcium binding.

Our findings expand the repertoire of CaM gymnastics on ion channels, and suggest a biophysical foundation for understanding an early step in the mechanism of calcium-mediated Na_V modulation. The available crystallographic structures of half-saturated CaM bound to IQ motifs from $Na_V1.2$ (4JPZ) and $Na_V1.5$ (4JQ0), and our solution studies of calcium-saturated CaM bound to the IQ motif of $Na_V1.2$ suggest that calcium regulates a 3-step transition by binding to CaM_N at intermediate calcium levels, and at higher levels, binding to CaM_C at the IQ motif, triggering its rotation around the IQ residues. The reversal of orientation of CaM_C would move CaM_N at the least, and might require release and re-association, allowing CaM molecules to interact elsewhere on Na_V such as at the inactivation gate ([39–44], other linkers within $Na_V1.2$, or its intracellular tails in a manner similar to CaM interactions with Ca_V channels [43–46])

2. Materials and Methods

2.1 Calmodulin

Full-length, wild-type CaM (paramecium sequence, 89% identical (131/148) to mammalian CaM) was overexpressed and purified as described previously[15, 47] with purity assessed by denaturing electrophoresis, UV/Vis spectroscopy and HPLC. Concentrations were determined using the BCA assay[48] (Pierce Biotechnology; Rockford IL) and by absorbance of denatured CaM in 0.1 M NaOH ($\varepsilon_{293.3}$ of 2330 $M^{-1}cm^{-1}$).[49]

2.2 YFP-CFP Biosensors Containing $Na_V1.2$ IQ

A biosensor pET21B vector expressing a gene for YFP upstream of a Kpnl site and CFP downstream of an AgeI site was a gift from A. Persechini and D.J. Black.[38, 50] A DNA oligomer optimized for bacterial expression and coding for the protein sequence of rat $Na_V1.2$ residues 1901 to 1927 (KRKQEEVSAIVIQRAYRRYLLKQKVKK) was purchased from Integrated DNA Technology (Coralville, IA) and inserted between the KpnI and AgeI sites (underlined residues constitute the canonical IQ motif sequence, IQxxx[R,K]Gxxx[R,K]). Overexpression in BL21(DE3) cells was induced by addition of IPTG; cultures grew for 40 hours at 18 °C. Cells were lysed at 4 °C by sonication for 80 s in 50 mM HEPES, 100 mM KCl, 50 03BCM EGTA, 5 mM NTA, 1 mM $MgCl_2$; pH 7.4 and clarified by ultracentrifugation (Beckman TI-60, 25K rpm, 45 min, 4 °C). Biosensor expression was verified by SDS-PAGE; concentration was determined by UV-Vis absorbance with ε_{514} of 83400 $M^{-1}cm^{-1}$.[51] CaM binding to biosensor in clarified cell lysate was indistinguishable from CaM binding to biosensor purified to homogeneity by nickel affinity chromatography.

2.3 Calmodulin Titrations of $Na_V1.2$ IQ Biosensors

The biosensor concentration ranged from 0.5 nM (for binding apo CaM) to 5 nM (for binding calcium-saturated CaM). Buffer was 50 mM HEPES, 100 mM KCl, 50 pM EGTA, 5 mM NTA, 1 mM $MgCl_2$; pH 7.4, 22 °C, with 1.5 μM BSA and 500 μM DTT. Calcium-saturating conditions included 1 mM $CaCl_2$. Titrations were conducted in a 1 cm Suprasil quartz cuvette (Hellma USA, Inc., Plainview, NY); the solution was stirred continuously with a Teflon stir bar in a water-jacketed cuvette-holder held at 22 °C on a QuantaMaster-4 Steady State Spectrofluorometer System with a xenon lamp (Photon Technologies International; New Jersey, USA). The sample was excited at 430 nm and emission spectra were collected from 450–550 nm. Peaks were observed at 475 nm (CFP) and 525 (YFP) nm. An experimentally determined isoemissive point (typically at 511 nm) was also monitored during the titration. Bandpasses were 4 nm for excitation and 8 nm for emission; integration time was 4 to 8 s after each addition of CaM delivered by positive displacement pipets (Drummond Wiretrol) from stocks representing 10-fold serial dilutions spanning 6 orders of magnitude, from pM to pM. Normalized isotherms were determined from the fractional change in YFP intensity (525 nm) corrected for dilution (based on intensity at the isoemissive wavelength); the net decrease in YFP intensity (Fig. 3A) differed for binding apo and calcium-saturated CaM.

2.4 Free Energy of CaM binding to $Na_V1.2_{IQ}$ Biosensors

Titrations were analyzed using nonlinear least squares analysis.[52] The fractional saturation ($\overline{Y}$) of the biosensor was described by Eq. (1) in which K_a, the association constant, is the reciprocal of K_d, the dissociation constant.

$$\overline{Y}=\frac{K_a \bullet [CaM_{\text{free}}]}{(1+K_a \bullet [CaM_{\text{free}}])} \quad (1)$$

To calculate $[CaM]_{free}$, the independent variables $[CaM]_{total}$ and $[biosensor]_{total}$ were used in an iterative convergence algorithm according to the quadratic equation described in Eq. (2) in which b is $(1 + K_a \cdot [biosensor] - K_a \cdot [CaM]_{total})$.

$$[CaM_{free}] = \frac{-b \pm \sqrt{b^2 - 4K_a(-[CaM_{total}])}}{2K_a} \quad (2)$$

Equation 3 accounted for experimental variations in the observed end points of individual titration curves:

$$\text{Signal} = f(X) = Y_{[X]low} + (\overline{Y} \bullet \text{Span}) \quad (3)$$

where $\overline{Y}$ refers to average fractional saturation of the biosensor and $Y_{[X]low}$ corresponds to the intrinsic fluorescence intensity of biosensor in the absence of CaM. The variable *Span* represents the magnitude and direction of signal change upon titration (i.e., the difference between the endpoints at high and low [CaM]). Following the signal of fluorescence intensity of YFP at 525 nm, the *Span* was negative for increasing additions of CaM. The endpoints were fit directly in analysis of all titrations.

The quality of the nonlinear least squares fit was evaluated by judging the square root of the variance, values of the 67% asymmetric confidence intervals, span and randomness of the distribution of residuals, and absolute values of elements of the correlation matrix.[53] The square root of the residual variance was typically less than 0.02. The magnitudes of the confidence intervals were within a factor of two of the standard deviation observed between independent, replicate titrations. All average free energy values reported in Table 1 were based on 4 to 9 replicate determinations from at least two preparations of biosensor overexpressed from independent bacterial colonies. For CaM_N, the deflection of YFP intensity was so small at high $[CaM_N]$ that it was not possible to estimate the affinity of CaM_N for the biosensor.

The change in normalized fluorescence intensity of CaM or CaM_C binding to the biosensor was simulated in Fig. 3 using Eq. (3) that accounted for the plateau intensity of free and CaM-saturated biosensor, as well as the decrease in intensity upon CaM binding. Free energies (and their corresponding equilibrium constants) are given in Table 1. Single-site isotherms of fractional saturation of the IQ motif by apo or calcium-saturated CaM (Fig. 7A) were simulated according to Eq. (1) and the values in Table 1.

2.5 Simulation of Calcium-Binding Isotherm

We previously measured energies of calcium binding to CaM alone under the conditions used in this study; in the absence of the IQ motif, AG_1 was −7.76 and ΔG_2 was −15.92 kcal/mol.[54] Based on the principle of conservation of energy (shown in the linkage equations below), the difference in energy between apo CaM (ΔG_a) and calcium-saturated CaM (ΔG_d) binding to the $Na_V1.2$ IQ biosensor (Table 1, $\Delta\Delta G$ +1.93) must be the same as the difference

in calcium binding to CaM alone (ΔG_c) and to CaM bound to the $Na_V1.2$ IQ biosensor ($206G_b$).

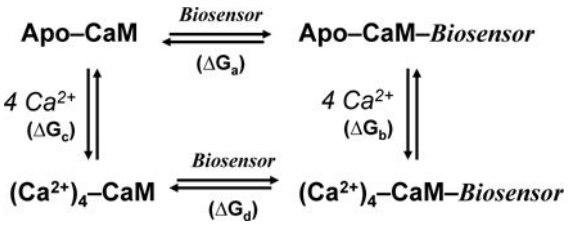

(4)

Thus, for illustration, we simulated a titration curve for calcium binding to sites III and IV of CaM bound to the $Na_V1.2$ IQ motif (in Fig. 7B) with a total free energy of −13.99 kcal/mol and the same cooperativity as observed for CaM alone.

2.6 NMR Samples

Uniformly labeled ^{15}N-CaM_C or ^{13}C,^{15}N-CaM_C was expressed in *E. coli* BL21(DE3) cells and contained a slight molar excess of commercially prepared peptide (GenScript, New Jersey). These represented $Na_V1.2$ IQ motif residues 1901–1927, as previously described for NMR determination of the structure (2KXW) of the complex of $Na_v1.2_{IQp}$ bound to apo CaM_C.[16] In NMR samples, [CaM] was 1.5 mM in buffer composition identical to that used previously[16] (10 mM imidazole, 100 mM KCl, 0.01% NaN_3, 50 03BCM EDTA, pH 6.8) in 90% H_2O/10% D_2O for amide-detected experiments or 100% D_2O otherwise. Calcium in matching buffer was added to a final concentration of 3.3 mM, to exceed the concentration of sites (2 per complex).

2.7 NMR Data Acquisition

All experiments were run on either a 500 MHz Bruker Avance II NMR spectrometer equipped with a TXI probe or an 800 MHz Bruker Avance II NMR spectrometer equipped with a TCI cryoprobe. All experiments for assigning both backbone and side chain resonances of the protein were collected at 500 MHz; experiments for assigning the unlabeled peptide, as well as all NOESY experiments, were collected at 800 MHz. All NMR spectra were processed using NMRPipe [55] and analyzed using both Sparky[56] and CCPN Analysis.[57] Chemical shift differences were calculated on the basis of arithmetic differences in chemical shift (H or N) between the two spectra. ΔH and ΔN were scaled by the gyromagnetic ratios of ^{1}H and ^{15}N (normalized to ^{1}H). The combined chemical shift difference, AS, was calculated as $\sqrt{\Delta H^2+(\Delta N \bullet 0.1013)^2}$.

2.8 NMR Resonance Assignments

Backbone spectra (HNCA, HN(CO)CA, HNCACB, HN(CO)CACB, HNCO, and HN(CA)CO) for CaM_C were analyzed in Sparky[56], and the resulting peak lists were submitted to the PINE server[58] for automatic backbone assignment. The results were

verified manually and corrected as necessary in Sparky. Backbone assignments were then imported into CCPN Analysis [57], which was used for all further assignments.

Side chain resonances were assigned using H(CCO)NH, C(CO)NH, and HCCH-TOCSY experiments, complemented by NOESY data for aromatic rings and methionine epsilons. Unlabeled peptide was assigned using $^{12}C,^{14}N$ filtered TOCSY (26 and 46 ms spinlock times) and $^{12}C,^{14}N$ double filtered NOESY (80 and 120 ms mixing times) experiments to suppress signals from labeled protein.[59–61] ^{13}C and ^{15}N edited NOESY spectra (120 ms mixing times), as well as a $^{13}C,^{15}N$ edited, $^{12}C,^{14}N$ filtered NOESY (140 ms mixing time, [62]), were peak picked and initial assignments were made for unambiguous and somewhat ambiguous crosspeaks (those with 3 or fewer possibilities).

Backbone and non-stereospecific side chain assignments of $(Ca^{2+})_2$-CaM_C were straightforward and nearly complete (91% of all protons). As indicated in Supplemental Table S2, 35 of 38 missing assignments are possibly degenerate methylene protons, excluding M_{76} for which only the epsilon methyl is observed. Assignment of the residues for unlabeled $Na_v1.2_{IQp}$ was more difficult due to chemical shift degeneracy and the lack of an isotopic label. No assignments were obtained for three residues at each end of the peptide (1901–1903 and 1925–1927). The remainder of the peptide, which contained all residues that contact CaM_C, was assigned with sufficient completeness for structure determination (77% of expected protons); 19 of 33 missing peptide assignments may have degenerate chemical shifts and many are in solvent-exposed side chains (Supplemental Table S3).

2.9 Structure Calculations

Initial restraints for structure calculations were generated in CCPN Analysis.[57] Distance restraints were made for all assigned NOEs, and shift matching was used to generate additional ambiguous distance restraints. NOEs were grouped into bins based on measured peak intensities. Dihedral angle restraints were generated for both the protein and peptide using the built in DANGLE routine[63]; a residue-by-residue comparison showed that average values for the protein were highly consistent with those determined using TALOS+. [64] Additionally, a set of hydrogen bond restraints was generated to constrain alpha helices.

High-resolution models were generated using traditional solution NMR techniques of combining distance constraints derived from NOESY spectra with backbone φ and 03C8 dihedral angles derived from chemical shifts. Initial rounds of structure determination were carried out with Aria/CNS[65, 66] using standard protocols and importing restraints directly from CCPN Analysis.[57] Intermediate structures were generated in Xplor-NIH[67, 68] or CNS.[66] The results were used to manually curate restraint tables in an iterative manner. Additional hydrogen bond restraints were included to constrain residues in alpha helices. To verify the validity of these restraints, an ensemble calculated with the hydrogen bond restraints removed yielded a somewhat lower resolution but otherwise similar structure, suggesting that this data is not significantly biasing the final result (data not shown). After multiple rounds of structure calculations, restraint and violation analysis suggested no further changes to the distance restraints. The final ensemble of structures was generated as follows.

An ensemble of 300 structures was generated using CNS [66] from an extended starting structure of calcium-free CaM_C using torsion angle dynamics, out of which the 20 with the lowest energies were retained. This stage used the default *anneal.inp* script and consisted of a brief initial minimization followed by 1000 steps of high temperature dynamics at 50000 K, 1000 steps of cooling from 2000 K to 0 K, and finally 2000 steps of minimization. For the 20 lowest energy structures from this calculation, calcium ions were then added and placed very roughly in the calcium-binding loops. An additional set of restraints for positioning the calcium ions was derived from a crystal structure of calcium-saturated CaM (1EXR.pdb)[69] and included in a further CNS [66] refinement protocol using Cartesian dynamics and consisting of 2000 steps at 2000K, 2000 cooling steps from 1000 K to 0 K, and finally 2000 steps of minimization. The final force constants used were 50 kcal mol^{-1} $Å^{-1}$ for distance restraints and 200 kcal mol^{-1} rad^{-2} for torsion angle restraints. CNS [66] reported no backbone dihedral angle violations greater than 2° and no distance violations greater than 0.2 Å in this final ensemble. Complete structure statistics are reported in Table 2.

The final structures have good Ramachandran statistics as determined by PROCHECKNMR [70] (Table 2 and Supplemental Fig. S2). For the entire ensemble of 20 structures, 99.6% of non-glycine residues fall in the most favorable or allowed regions of torsion angle space (100% for the minimized average structure). All residues falling in the generously allowed (0.35%) and disallowed (0.05%) regions correspond to either Q_{1904} or K_{1924} which are only partially assigned and are at the disordered ends of the peptide. The PROCHECK-NMR [70] analysis omitted residues 76–78 and 148 in CaM_C, which were poorly ordered, and residues 1901–1903 and 1925–1927 in $Na_v1.2_{IQp}$, for which no NMR data or restraints are available.

All molecular models were drawn with PyMOL Molecular Visualization System v. 1.7.2.3 (Schrödinger, LLC).

3. Results

3.1 FRET Intensity of CaM-Biosensor Assemblies

To evaluate separable roles of CaM domains in recognition of the $Na_V1.2$ IQ motif, and to estimate equilibrium binding constants for both apo and calcium-saturated CaM and its domains, we monitored CaM-induced disruption of FRET in a biosensor protein[38, 50] that was engineered to contain the desired $Na_V1.2$ sequence (residues 1901–1927) bracketed by YFP and CFP (see Methods). Steady-state emission spectra (λ_{ex} = 430 nm) for the $Na_V1.2_{IQ}$ biosensor alone (green, 4 nM) with λ_{max} at 475 nm for CFP and 525 nm for YFP are shown in Fig. 3A.

FRET intensity is sensitive to small changes in distance between fluorophores induced by CaM binding to the IQ motif sequence in the $Na_v1.2_{IQ}$ biosensor. We have shown previously that the IQ motif sequence is intrinsically disordered.[15] This allows CFP and YFP to be in close proximity for efficient non-radiative transfer of energy. The typical change in intensity of the biosensor after saturation with apo (black, dashed) or calcium-bound (black, solid) CaM is shown in Fig. 3A ([CaM]:[biosensor] = 10^3:1). The emission spectra were buffer-subtracted and corrected for dilution; the spectra were normalized to the peak intensity of

free biosensor at 525 nm. The intrinsic fluorescence of CaM (which contains Phe and Tyr, but not Trp) does not contribute measurably to the intensities observed.

At λ_{max} for YFP, the fractional decrease in intensity was consistently larger for saturation by apo CaM (36±1%) than $(Ca^{2+})_4$-CaM (21±1%). We infer that apo CaM and $(Ca^{2+})_4$-CaM differ in conformation when bound to the IQ motif, and thus differentially reduce energy transfer from CFP to YFP by changing their relative orientation or spatial separation. The isoemissive point for free and CaM-saturated biosensor was observed consistently at 511 nm throughout the titration, indicating that it behaved as a two-component solution.

3.2 Domain-Specific Binding of CaM

To investigate whether both domains of CaM were necessary for the change in fluorescence intensity seen upon binding full-length CaM, a C-domain fragment (CaM_C, residues 76–148) or an N-domain fragment (CaM_N, residues 1–75) was added to the $Na_v1.2_{IQ}$ biosensor (4 nM) in large excess ([CaM]:[biosensor] = 10^3:1). The emission spectra of the $Na_v1.2_{IQ}$ biosensor with apo and calcium-saturated CaM_C bound (data not shown) were very similar to those in Fig. 3A for full-length CaM. However, Fig. 3B showed a negligible change (~1%) in intensity of the $Na_v1.2_{IQ}$ biosensor after addition of apo CaM_N (dashed blue), and a net change of ~3% for calcium-saturated CaM_N (solid blue) at a concentration of 15 03BCM CaM_N. The deflection in fluorescent intensity at 50 pM CaM_N was less than 1% of that seen at 50 nM CaM_C, showing high specificity for CaMC. These results are consistent with our prior studies using fluorescence anisotropy to study CaM and its domains binding to a fluorescein-labeled peptide corresponding to the same $Na_v1.2$ IQ motif sequence [15, 16]

3.3 Energetics of CaM Binding

Thermodynamic linkage analysis previously showed that apo CaM binds more favorably than calcium-saturated CaM to rat $Na_v1.2_{IQp}$.[14–16] However, the free energies of binding could not be determined quantitatively because the high concentration of $Na_v1.2_{IQp}$ needed to obtain sufficient signal in fluorescence anisotropy or gel electrophoresis mobility shift experiments resulted in stoichiometric titrations. In contrast, the strong fluorescence intensity of the $Na_v1.2_{IQ}$ biosensor permitted titrations to be conducted at concentrations as low as 0.5 nM (see Methods). The fractional change in intensity at λ_{max} for YFP (normalized to biosensor alone at 100% and CaM-saturated biosensor as zero) was plotted as a function of total concentration of added CaM or CaM_C, under either apo (Fig. 3C), or high calcium (1 mM, Fig. 3D) conditions.

These binding isotherms allowed direct estimates of Gibbs free energies of binding (AG) and corresponding dissociation constants (K_d) under equilibrium conditions (Table 1). Apo CaM binding to the $Na_v1.2_{IQ}$ biosensor (−11.48 kcal/mol (K_d 3.2 nM) was more favorable by −1.93 kcal/mol than the binding of calcium-saturated CaM (−9.55 kcal/mol; K_d 85 nM). The difference was significantly larger than the standard deviations (0.18 and 0.08 kcal/mol) of multiple replicate titrations for apo and calcium-saturated CaM, respectively. The difference similarly exceeded the confidence intervals for individual determinations (median

value of 0.10 kcal/mol), and suggested that the interface between apo CaM and the IQ motif changed when sites III and IV filled with calcium.

Because CaM_N showed negligible binding to the $Na_v1.2_{IQ}$ biosensor (Fig. 3B), it was not possible to observe a titration or estimate a free energy of interaction. However, to visually compare its behavior to that of CaM and CaM_C under apo (Fig. 3C), or high calcium (1 mM, Fig. 3D) conditions, the small change in intensity observed upon addition of CaM_N was normalized by assuming that the YFP signal of the biosensor would undergo the same deflection as observed for CaM (i.e., 36% for apo and 21% for calcium-saturated CaM) if it were saturated by CaM_N. Even if the slight deflection observed at 10 03BCM CaM_N were attributable to specific binding rather than non-specific quenching, the midpoint of a complete titration would be higher than 100 03BCM, corresponding to a very weak dissociation constant. It is also possible that this modest binding represents CaM_N binding to the same Na_V sequence that is occupied by CaM_C when full-length CaM is bound, and thus represents an interaction that would not be populated in the cell where only full-length CaM is available. We observed a similar phenomenon for domain-specific binding of CaM to melittin.[71]

3.4 CaM_C Binding to $Na_v1.2_{IQp}$ Independent of CaM_N

The titrations in Fig. 3 indicated that the driving force for CaM binding to the IQ motif comes primarily from residues in the C-domain of CaM. Although the binding of CaM_C was slightly less favorable than CaM for each condition (see Table 1), this may reflect electrostatic differences in attraction for the very basic $Na_v1.2_{IQ}$ sequence, rather than differences in close contacts such as van der Waals interactions or hydrogen bonding at the interface of CaM and $Na_v1.2_{IQp}$. The calculated net charge at pH 7 (http://www.scripps.edu/~cdputnam/protcalc.html) of CaM is −23.5 and CaM_C is −12.6. Approximating CaM and CaM_C as negative point charges binding to positive IQ motifs, the Coulombic contributions (proportional to q_1*q_2/r^2 [72]) to their free energies of binding to the IQ motif would differ by the square of the ratio of their charges (23.5 vs. 12.6), or a factor of ~4. That represents a free energy of $-RTln(4)$ or .813 kcal/mol at 22 °C which corresponds well with the ΔΔG values of 0.76 and 0.89 kcal/mol reported in Table 1.

To assess directly whether the CaM-peptide interface was the same for $(Ca^{2+})_4$-CaM-$Na_v1.2_{IQp}$ and $(Ca^{2+})_2$-CaM_C-$Na_v1.2_{IQp}$, HSQC spectra of ^{13}C,^{15}N-labeled complexes of $(Ca^{2+})_4$-CaM (black) and $(Ca^{2+})_2$-CaM_C (red) bound to $Na_v1.2_{IQp}$ were compared (Fig. 3E). The green ellipses encircle resonances for the same residue in each complex, and show that they are in identical or nearly identical positions, indicating that their chemical environment is very similar. Resonances in the highly overlapped central region boxed by a dashed line are shown in an enlarged format in Fig. 3F.

Consistent with the interface between $Na_v1.2_{IQp}$ and CaM being dominated by close contacts with CaM_C, resonances within the N-domain of $(Ca^{2+})_4$-CaM bound to the $Na_v1.2_{IQ}$ peptide matched those in a free fragment $(Ca^{2+})_2$-CaM_N (see Supplemental Figure S2). These studies match prior NMR studies showing that CaM binding $Na_v1.2_{IQp}$ caused few perturbations of residues within the N-domain of either apo or calcium-saturated CaM. [16].

Therefore, to determine why $(Ca^{2+})_2$-CaMC binds less favorably than apo CaMC to the $Na_V1.2$ IQ motif, and understand how calcium binding changes the interface between CaM_C and the $Na_V1.2$ IQ motif without the influence of auxiliary proteins or flanking regions, we determined a high resolution structure of CaM_C bound to a peptide representing the IQ motif (hereafter referred to as the CaM_C-$Na_v1.2_{IQp}$ complex). NMR allowed determination of the complex in solution without packing constraints that might be contributed by a crystallographic lattice.

3.5 Solution structure of Ca^{2+}-CaM_C bound to $Na_v1.2_{IQp}$

The structure was determined using a sample of $^{13}C,^{15}N$-$(Ca^{2+})_2$-CaM_C bound to unlabeled $Na_v1.2_{IQp}$ (see Methods). Nearly complete assignments of CaM_C and central $Na_v1.2_{IQp}$ peptide residues that interact with CaM_C were obtained (see Supplemental Tables S2 and S3). Backbone traces of the 20 NMR-derived lowest energy structures of the complex are superimposed in Fig. 4A in two orientations: with $Na_v1.2_{IQp}$ perpendicular and parallel to the plane of the figure. The Ramachandran plot is in Supplemental Figure S3; Table 2 provides structural statistics. In the minimized average NMR structure of the complex (Fig. 4B), $(Ca^{2+})_2$−CaM_C adopts a 4-helix bundle in the classic open conformation (see Fig. 2A), with side chains in the EF-hand sites consistent with the metal-coordination geometry adopted when calcium is bound (see Supplemental Fig. S1B). Residues 1904–1923 of $Na_v1.2_{IQp}$ form an amphipathic α-helix closely associated with $(Ca^{2+})_2$-CaM_C. The terminal residues (1901–1903, 1924–1927) of $Na_v1.2_{IQp}$ were disordered, as had been observed for $Na_v1.2_{IQp}$ bound to apo CaM_C.

Analysis of the minimized average structure with CSU (Contacts of Structural Units [73]) in Fig. 4C showed residues in $Na_v1.2_{IQp}$ (bottom row) that are in the binding interface with CaM_C, and the vertical stacks show CaM_C residues that have atoms within 6 A of $Na_v1.2_{IQp}$; contacts that were ≤ 4.5 Å are shaded orange.

The side chains V_{1911}, I_{1912}, A_{1915} and Y_{1916} (Fig. 4B) make many contacts with the hydrophobic cleft of CaM_C, including the FLMM residues (F92, L112, M124, M144) observed to bind a large number of peptides in calcium-saturated CaM_C complexes ([74–76]). Residue Q_{1913} in the IQ motif of $Na_v1.2_{IQp}$ points towards the C-terminus of CaM_C.

For determining the orientation of CaM_C relative to the peptide, the key intermolecular NOEs observed between CaM_C and $Na_v1.2_{IQp}$ were those associated with CaM_C residues A88, V91 and M124 (Fig. 4D). $Na_v1.2_{IQp}$ has only two aromatic residues (Y_{1916} and Y_{1919}) with distinct chemical shifts, each of which makes unambiguous NOE contacts to both A88 and V91. The side chain of A_{88} comes within 2.4 Å of Y_{1916} (vs. 7.8 Å in 2KXW), and the V_{91} side chain is within 3 Å of Y_{1919} and just over 5 Å from Y_{1916} (both >10 Å in 2KXW). Furthermore, the side chain of M_{124} makes contacts with Hα and both Hβs of S_{1908}, which is the only serine in $Na_v1.2_{IQp}$ and more than 11 A away from M_{124} in the corresponding apo structure (2KXW).

To see the overall effect of peptide binding on $(Ca^{2+})_2$-CaM_C, a ^1H-^{15}N HSQC of $(Ca^{2+})_2$-CaM_C bound to $Na_v1.2_{IQp}$ was compared to a corresponding spectrum of $(Ca^{2+})_2$-CaM_C alone (Fig. 5A). The chemical shift perturbations observed for each backbone amide upon

binding to $Na_v1.2_{IQp}$ localized mainly in helices E, F, and H (Fig. 5B) and the largest differences in chemical shift were in regions contacting $Na_v1.2_{IQ}$ (Fig. 5C). The resonances for residues within sites III and IV in these two samples were nearly identical regardless of the peptide binding, suggesting that the geometry of calcium-chelation is also identical. As noted in Methods, NMR does not directly visualize the position of metal ions. Therefore, the positions of calcium ions shown in Fig. 5C were fit based on the side chain geometry of highly acidic coordinating residues. Such residues would undergo electrostatic repulsion if there were no divalent cation present.

3.6 Reversal of CaM_C on the IQ motif

The most striking feature of the solution structure (2M5E) of calcium-saturated CaM_C bound to $Na_v1.2_{IQp}$ was the orientation of $(Ca^{2+})_2$-CaM_C relative to $Na_v1.2_{IQp}$. According to the NOEs shown in Fig. 4D, it was opposite to that observed in apo CaMo-$Na_v1.2$IQp in 2KXW.[16] A nearly 180° rotation of a CaM domain on the same hydrophobic face of a target CaMBD helix was an unexpected response. The protein samples used for determining 2M5E were made by adding excess calcium to an equilibrated complex of apo CaM_C bound to $Na_v1.2_{IQp}$ that was from the same stock used for determining 2KXW (see Methods). Thus, the final structure shown in Fig. 4 required that (Ca^{2+})2-CaMC either pivoted in place, or released and re-associated with $Na_v1.2_{IQ}$.

In both 2M5E and 2KXW, the sequence of $Na_v1.2_{IQ}$ was sufficiently long to encompass residues that interact closely with CaM_C as well as containing terminal residues (1901–1904 and 1924–1927) that were non-interacting and highly disordered. Thus, the $Na_v1.2_{IQp}$ sequence appeared to bracket residues needed for tight binding to CaMC. The comparison of HSQC spectra of $(Ca^{2+})_2$-CaM_C and apo CaM_C, each in complex with unlabeled $Na_v1.2_{IQp}$ (Fig. 6A), showed that few CaM resonances overlapped. A comparison of ^{12}C,^{14}N filtered NOESY spectra for both apo and calcium-saturated CaM_C-$Na_v1.2_{IQp}$ complexes (partial spectra shown in Supplemental Figure S4) shows striking differences consistent with calcium binding inducing a major conformational change as represented in Fig. 4 and 5.

Some changes in peak positions reflect the expected effects of calcium occupancy of sites and the opening of the tertiary structure triggered by calcium binding (i.e., semi-open to open conformation) that would occur for CaM alone. However, spectral comparisons of calcium-saturated $CaM_C \pm Na_v1.2_{IQp}$ in Fig. 5A showed that binding of the peptide made additional changes in CaM peaks beyond those caused by calcium binding. The magnitude and direction of the perturbations seen in Fig. 6A reflect binding of calcium at sites III and IV, and binding of $Na_v1.2_{IQp}$ in the open cleft of CaM_C.

The chemical shift perturbation for each resonance that was assigned in both 2KXW and 2M5E (Fig. 6B) showed many large changes between the structures (average Δ03B4 of 0.5 ppm). With a false-color scale of red (representing greatest) to blue (least) perturbation, Fig. 6C highlights that the major differences outside calcium-binding sites III and IV were in the FG-linker which changes contacts dramatically when CaM_C pivots relative to $Na_v1.2_{IQ}$. Consistent with analysis of short-range structural contacts (Fig. 4C) in $(Ca^{2+})_2$-CaM_C (2M5E), residues in the CaM_C FG-linker contact A_{1915} in $Na_v1.2_{IQp}$ whereas in apo CaM_C (2KXW), the FG-linker made a network of hydrogen bonds with Q_{1913}. Because of the

reversal of $(Ca^{2+})_2$-CaM_C on $Na_v1.2_{IQp}$, Q_{1913} in 2M5E primarily contacts residues near the C-terminus of CaM and the residues that would be closest to CaM_N.

Fig. 6D and 6E (90° rotations) show 2M5E and 2KXW aligned according to the backbone of $Na_v1.2_{IQp}$. Positions of selected side chains (I_{1912}, Q_{1913}, A_{1915}, Y_{1916} and Y_{1919}) that make multiple contacts with CaM are shown in ball-and-stick format. CaMC residue 76 (blue) indicates the junction with CaM_N, highlighting the reversal of CaM relative to the channel peptide. The open conformation of $(Ca^{2+})_2$-CaM_C (2M5E) (Fig. 6D) has a more shallow hydrophobic cleft than the semi-open conformation of apo CaM_C (2KXW). A view looking into the clefts (Fig. 6E) shows that in apo CaM_C (2KXW), the side chains of I_{1912}, Q_{1913}, A_{1915}, Y_{1916} are tightly clustered in the deep semi-open cleft whereas these residues are distributed over a wider surface of the hydrophobic cleft in 2M5E, with Y_{1916} oriented closer to Y_{1919} in the calcium-saturated structure.

Although the rotation of $(Ca^{2+})_2$-CaM_C on $Na_v1.2_{IQp}$ was unexpected, the observed polarity of $Na_v1.2_{IQp}$ relative to CaM_C is consistent with hundreds of other complexes of calcium-saturated CaM bound to peptides representing CaMBDs from other ion channels, receptors and enzymes (see Fig. 2A). These motifs are commonly denoted by a numbering scheme (such as 1–5–8) indicating the positions of residues in the primary sequence that interact closely with CaM clefts. In 2M5E, $Na_v1.2_{IQp}$ residues I_{1912}–Y_{1916}–Y_{1919} correspond to positions 1–5–8 in a typical motif, and I_{1912} is the sole residue contacting all 4 of the FLMM residues [75] in CaM_C.

4. Discussion

CaM is an essential, intracellular, eukaryotic calcium sensor that regulates both aqueous and membrane-spanning target proteins. In turn, those targets are allosteric effectors of the calcium-binding free energies of CaM, making CaM an effective modulator over a range of intracellular calcium concentrations that spans at least three orders of magnitude, bracketing its micromolar affinity for calcium as a free protein.[77, 78] Voltage-dependent sodium channel $Na_V1.2$ retains CaM as a constitutive subunit, but the mechanism of calcium-triggered change in the complex has been perplexing because previous structural studies did not see calcium bound to CaMC which anchors CaM to the channel.

4.1 All IQs are BAAs, But Not All IQs are Equal

The magnitude and direction of a target-linked shift in calcium-binding affinity of CaM and its conformational response when bound to a target is not predictable from the CaMBD sequence alone. All known CaMBDs are BAAs - Basic sequences (pl of 10–12) that form Amphipathic Alpha helices (usually continuous). Many bind exclusively to the open conformation of domains in $(Ca^{2+})_4$-CaM, with no measurable affinity for apo CaM. Others, such as the NMDA receptor [79] and phosphodiesterase [80], retain apo CaM as a constitutive subunit but have a higher affinity for calcium-saturated CaM than apo CaM which binds primarily via contacts with CaM_C. Calcium binding to CaM_N changes the mode of interaction of CaM with the target protein.

The set of target proteins that binds the semi-open cleft of apo CaM domains more favorably than the open cleft of calcium-saturated CaM domains include neuromodulin [81–83] and neurogranin [82, 84] as well as some myosins. Their CaMBDs are IQ motifs, a subclass of BAA motifs, and some release CaM when calcium binds CaM.[85] Sequence variations flanking the IQ motif influence whether only CaM_C, or both domains of CaM, interact with the IQ motif.[27, 86–88]

For the well conserved IQ motifs in human voltage-gated sodium channels, NMR and crystallographic studies of CaM binding to $Na_V1.2$, 1.5, and 1.6 have shown that apo CaM_C anchored CaM on the IQ motif, while apo CaMN adopted variable positions and made few contacts with the channel fragment. This was consistent with thermodynamic data that showed undetectable or very weak binding to these IQ motifs by CaM_N. Through linkage or direct thermodynamic measurements, these studies also showed that the Na_V IQ motifs have a higher affinity for apo CaM than $(Ca^{2+})_4$-CaM.[15, 16, 22, 33, 41] These studies of Na_V-CaM interactions contrast with the behavior of IQ motifs in voltage-dependent calcium channels such as $Ca_V1.2$, which interacts with both domains of CaM and has a higher affinity for $(Ca^{2+})_4$-CaM than apo CaM [89–91], despite the similarities between the calcium and sodium channels.[92]

4.2 Apo and $(Ca^{2+})_4$-CaM binding to $Na_V1.2$ IQ

The IQ-motif of $Na_V1.2$ binds both apo CaM and $(Ca^{2+})_4$-CaM with high affinity (Table 1). In our earlier studies of CaM binding to a fluoresceinated peptide of the $Na_V1.2$ IQ motif, the stoichiometric conditions required for signal-to-noise ratios that yielded reproducible measurements allowed us only to put limits on the dissociation constants because the K_d was similar to, or much lower than, the concentration of peptide being titrated. This challenge of estimating dissociation constants plagues many biophysical methods such as quantitative mobility shift assays and isothermal titration calorimetry where it can be impossible to detect a concentration of macromolecule that is an order of magnitude lower than the value of the K_d, leading researchers to conduct studies under stoichiometric conditions.

To address the low spectral intensity inherent in our prior studies using fluorescence anisotropy, here we employed the biosensor method of Black and Persechini.[38] The high steady-state intensity of YFP-CFP FRET allowed titrations to be conducted biosensor concentrations as low as 0.3 nM biosensor, a factor of 10 lower than the most favorable observed K_d. Although it would have been preferable to use an even lower concentration of biosensor, in the nonlinear least squares analysis to determine free energies, the difference between free and total [CaM] was accounted for by using a function that calculated free [CaM] from the total [CaM] and the degree of saturation (see Methods).

Simulations of saturation of the $Na_V1.2$ IQ motif based on the AG values reported in Table 1 for apo (dashed) and calcium-saturated (solid) CaM are shown in Fig. 7A. The 30-fold separation in midpoints indicates that the CaM-IQ interface must be different, but a small conformational change that resulted in the loss of a few hydrogen bonds might account for this weakening of affinity for $(Ca^{2+})_4$-CaM. Instead, our solution structures 2KXW and 2M5E (insets in Fig. 7A) showed that calcium triggers an ~180° rotation of CaM_C around I_{1912} in the IQ motif, causing many changes at the binding interface between CaM_C and

residues in the IQ motif. The final conformation is similar to that of CaM_C in $(Ca^{2+})_4$-CaM bound to peptides from a variety of targets such as $Ca_V2.2$ (3DVJ [27]), CaMKl (1MXE [93]), and $Na_V1.5$ III–IV linker (4DJC [40]).

To infer the biological occupancy of an IQ motif by one of the endstates of CaM (with 0 or 4 calcium ions bound), it is essential to know both the equilibrium constants for binding the IQ motif and the local cellular concentration of free CaM. In cells, the level of CaM will depend on the expression levels of target proteins and their post-translational modifications, as well as the affinity of CaM for each target.[32, 83, 94–97] The affinity is also a function of the degree of calcium occupancy of CaM. To infer binding occupancy of the $Na_V1.2$ IQ motif, we estimated free [CaM] as 50–100 nM.[97, 98] Fig. 7A shows that this would correspond to 94–97% occupancy by apo CaM, and 37–54% occupancy by (Ca^{2+})4-CaM. This predicts that, regardless of the level of free calcium, CaM would be constitutively bound to the $Na_V1.2$ IQ motif. This prediction agrees with proteomics studies of $Na_V1.2$-associated proteins in neuronal cells, which found the level of enrichment of CaM in $Na_V1.2$ pull-downs to be similar to that of other constitutively interacting proteins such as the Na_V β2 subunit and FGF12 (FHF1).[11]

4.3 States of CaM-IQ: 0, 2, or 4 Ca^{2+}

A cell experiences increases in calcium concentration due to release of calcium from internal stores or influx from the extracellular space. A calcium titration in a cuvette or NMR tube mimics this transition. Titrations of CaM-IQ_p monitored by NMR showed that calcium bound to CaM with a stoichiometry of 4 ions to 1 CaM.[16] However, the calcium-binding affinity of sites III and IV (CaM_C) was diminished, while the affinity of sites I and II (CaM_N) was similar to those sites in free CaM.[16] Thus, the CaM domains behave differently and may bind calcium sequentially but the CaM-IQ_p complex can attain full saturation with 4 calcium ions bound.

Crystallographic structures of an intermediate state having half-saturated CaM bound to the IQ motifs of $Na_V1.2$ (4JPZ) or $Na_V1.5$ (4JQ0) provide insight into the transition during a calcium influx. Both structures have calcium bound to sites I and II in CaM_N, while sites III and IV are not saturated. The 4-helix bundles of CaM_C in 4JPZ and 4JQ0 retain the semi-open tertiary conformation and orientation characteristic of apo CaM bound to the IQ motifs of $Na_V1.2$ (2KXW) and $Na_V1.5$ (2L53, 4DCK, and 4OVN) shown in Fig. 2. These are similar to the groundbreaking structure (1G4Y, Fig. 2E) of CaM bound to a large fragment of the SK channel [20] in which CaM_C was apo, while CaM_N was calcium-saturated.

The full ensemble of populated states of $Na_V1.2$ changes in response to the abundance of both CaM and calcium. In this study, we did not directly measure calcium binding to the complex containing CaM bound to the $Na_V1.2$ IQ motif. However, we can simulate this behavior based on the difference in free energy (ΔΔG) of binding apo and calcium-saturated CaM to the $Na_V1.2$ IQ motif (1.93 kcal/mol in Table 1). Applying the principle of thermodynamic linkage, this value of ΔΔG must be the same as the difference between the AG of calcium binding to free CaM and to the apo CaM-$Na_V1.2$ complex. The simulation in Fig. 7B represents predicted occupancy of the $Na_V1.2$ IQ motif by $(Ca^{2+})_4$-CaM.

Because the K_d for $(Ca^{2+})_4$-CaM binding to the IQ motif is ~30-fold higher (weaker) than that of apo CaM, the preferred binding partner for $Na_V1.2$ at resting calcium conditions is apo CaM, which is depicted schematically in the blue vertical bar. The green bar signifies high calcium; at 10 03BCM free calcium, occupancy of the IQ motif by $(Ca^{2+})_4$-CaM would be ~68% or two-thirds. While 10 03BCM free calcium does not persist in cells for long periods of time, and does not occur uniformly throughout the cell, the level of calcium may rise to this level transiently and locally in nanodomains.[99]

4.4 Rotation in Place

A schematic diagram depicting the transition from 0 to 2 to 4 calcium ions bound to CaM when associated with the $Na_V1.2$ IQ motif is shown in Fig. 7C. In this model, calcium binding to sites I and II affects only CaM_N, while calcium binding to sites III and IV triggers reversal of CaM_C orientation on the IQ motif. Our NMR data for apo and calcium-saturated CaM bound to $Na_v1.2_{IQp}$ showed that backbone resonances for residues in CaM_N in the CaM-IQ_P complex and free CaM_N were essentially identical (Supp. Fig. S2) indicating that CaM_N does not bind to $Na_V1.2_{IQP}$. This independence of CaM_N was also seen in the NMR structure (2L53, Fig. 1E) of apo CaM bound to $Na_V1.5$. Thus, in Fig. 7C, CaM_N is represented as a free domain, without a preferred interface on $Na_V1.2$.

However, apo CaM_N might adopt positions similar to the two distinct, and well-separated locations seen in the crystallographic structures for apo CaM_N bound to $Na_V1.5$ (4OVN or 4DCK, Fig. 1E), while calcium-saturated CaM_N may adopt a position similar to those seen in structures 4JPZ or 4JQ0. The reversal of CaM_C occurs with or without CaM_N. Future studies in solution of CaM binding to a longer fragment of $Na_V1.2$ will be required to address to what extent the positions of CaM_N observed in crystallographic studies represent energetically preferred orientations that are persistent in cells.

This simple 3-state model provides CaM with a vocabulary of at least three words for allosteric regulation of $Na_V1.2$. The larger question is how these might align with three functional states of the channel broadly defined as closed, open and inactivated. However, each of those functional states is much more complex than a single protein conformation, and the physiological complexes include the Na_V β subunits (with a single transmembrane helix), as well as auxiliary intracellular proteins such as intracellular FGFs (FHFs), ankyrins, CaMKII, synaptotagmin, and casein kinase II β which are also thought to modulate the Na_V α subunit.[100, 101] Although our data cannot directly address the correlation between energetically accessible structures and physiological regulation of $Na_V1.2$, they provide a striking new insight into an unexpected structural response to calcium binding, and suggest that it will be worth determining to what degree the calcium-saturated state observed in 2M5E is populated in cells.

4.5 Structural Correlates of 3-State Switch

CaM-target structures representing the 3 states depicted schematically in Fig. 7C are shown in Fig. 7D. They were aligned using PyMOL (Schrödinger, LLC) according to the positions of residues corresponding to residues 1909–1915 of $Na_V1.2$ in 2M5E, where I_{1912} (cyan) and Q_{1913} (green) in $Na_V1.2$ are shown as ball-and-stick, and residues at positions

corresponding to those IQ residues are represented the same way in the other structures. To highlight the orientation of CaM, CaM_C helices E and H are gray, while F (red) and G (orange) draw attention to the reversal of CaM_C relative to I_{1912} and Q_{1913}. Apo CaM bound to the $Na_V1.5$ IQ motif (4OVN) and to an IQ motif of myosin V (2IX7) show that the eponymous Q side chain is oriented towards the FG-linker in semi-open apo CaM_C as it is in 2KXW. The intermediate state of CaM (having two calcium ions bound to CaM_N) associated with the $Na_V1.2$ IQ motif (4JPZ) retains the same orientation of CaM_C relative to the IQ motif as the apo form of CaM.

A recent report [102] of a calcium-triggered reversal of CaM_C on IQ motif 1 of myosin V (4ZLK), shown in the right panel of Fig. 7D, is similar in orientation to 2M5E. In both structures, calcium binding to CaMC triggers opening and reversal of the 4-helix bundle, with the side chain of Q oriented towards the linker between CaM_N and CaM_C. The observed polarity of $Na_v1.2_{IQp}$ relative to CaM_C is consistent with most other complexes of calcium-saturated CaM bound to peptides [32] representing CaMBDs from other ion channels, receptors and enzymes such as CaMKII (1CDM) shown in Fig. 2A (termini of the CaMBD peptide (green) are indicated in blue/N and red/C).

4.6 Reversal by Release and Recapture

How CaM could regulate Na_V channels while remaining very tightly bound to “one” site within the C-terminal tail has been a long-standing conundrum. The thermodynamic and structural studies presented here demonstrate that calcium binding reverses the polarity of CaM bound to the $Na_V1.2$ IQ motif because CaM_C recognizes nested, anti-parallel sites within a single helix in a calcium-dependent manner. This unexpected re-orientation of CaM illustrates the exquisite power of calcium-induced helical reorientations to result in large re-orientation of CaM to yield regulatory effects. Although studies here only addressed interactions of CaM with the IQ motif of $Na_V1.2$, they suggest several hypotheses about the regulatory action of CaM on the channel as a whole. Because calcium binding to CaMC triggers it to rotate in the saddle of the hydrophobic face of the IQ motif, this might assist in modulating $Na_V1.2$ by moving CaM_N into an alternative position that could reach other sequences within $Na_V1.2$ or its auxiliary regulatory proteins. Based on studies of CaM-NaV interactions, Young and Caldwell postulated that $Na_V1.4$ might contain an NLBD – a non-IQ domain that binds CaM_N.[101]

The observed calcium-induced reversal of CaM also provides a plausible mechanism for transient release of CaM from the $Na_V1.2$ IQ motif, despite its very high affinity for both apo and calcium-saturated CaM. This would be analogous to IQCG (IQ motif-containing G protein) in which calcium causes release of CaM_C but promotes binding of $(Ca^{2+})_2$-CaM_N. [103] Although none of the experiments reported here directly address the kinetic aspects of binding or release of CaM from the channel or the IQ motif, Fig. 7E illustrates some plausible models based on known CaM-target interactions. One study concluded that dissociated $(Ca^{2+})_4$-CaM acts on $Na_V1.5$ indirectly by binding to CaMKII which then phosphorylates the channel.[101] Other studies of $Na_V1.5$ have proposed that high levels of calcium may cause CaM to release from the IQ motif and relocate at least one of its domains to the DIII-DIV linker, which has micromolar affinity for CaM_C.[39, 41] For $Na_V1.5$,

$(Ca^{2+})_4$-CaM binds at the DIII-DIV linker ("inactivation gate") through CaM_C as shown in the crystallographic structure 4DJC, which has the same polarity of CaMC-peptide interaction observed in many other calcium-saturated CaM complexes such as 1CDM (Fig. 2A). Given that the structure of the CTD of $Na_V1.5$ (4OVN, 4DCK, 4JQ0) is highly similar to the CTD of $Na_V1.2$ (4JPZ), release of $(Ca^{2+})_4$-CaM from the IQ motif might result in one or both CaM domains binding the $Na_V1.2$ DIII-DIV linker, post-IQ or other non-IQ CaM-binding sites within the CTD. Precedents exist for CaM binding the N-terminal tail of Ca_V channels [44, 45]; Na_Vs may have a similar site. $(Ca^{2+})_4$-CaM may bind to the NaV β subunits or other auxiliary proteins such as those depicted in models of $Na_V1.5$.[104]

Re-association or relocation of $(Ca^{2+})_4$-CaM might occur as it does for the STRA6 receptor for retinol uptake in which the two domains of CaM bind and bridge distinct sequences in the receptor that are not found in a continuous helix.[105] This was also observed for CaM binding to non-inactivating voltage-dependent KCNQ potassium channels.[106] Another plausible arrangement might follow the example of CaM binding to the SK Channel (1G4Y[20]) wherein a second CaM molecule may be recruited to $Na_V1.2$ when calcium levels rise. Such a mechanism would share features with the calcium-induced remodeling of myosin V, where one CaM molecule has been observed to bind two IQ motifs simultaneously.[85]

4.7 CaM-regulated Channels across Phyla

By studying Paramecium — a "unicellular neuron" — Kung and colleagues first discovered that CaM was a constitutive subunit of some calcium-regulated sodium and potassium channels, and that defects in each domain of CaM compromise a unique set of physiological responses to external stimuli.[107–110] Under-reactive mutants of this excitable cell deviated from wild-type CaM at positions in CaM_N that were primarily outside of the calcium-binding sites, while over-reactive mutants had changes in CaMC that were primarily localized within sites III and IV. Similar domain-specific results were later observed in mutagenic studies in yeast.[111] Exome analyses of humans have identified calmodulinopathies that are also specific to one domain of CaM.[112–115] Some of the identified positions, such as D95 in site III, have been found to be deleterious in both Paramecium and human studies, suggesting that their mechanisms of action are conserved.

Given that the sequences of Paramecium and human CaM are 89% identical, and 96% similar, and that all of the mutants identified by Kung were at positions that are identical in the human and Paramecium wild-type CaM sequences, it was predictable that the initial discovery of CaM-regulated ion channels would generalize to several families of calcium-regulated ion channels in all eukaryotes.[92, 116–119] For many of these channels, CaM is associated under resting (low calcium) conditions as it is with $Na_V1.2$. CaM may activate, inhibit, or do both, depending on its fractional saturation by calcium. For example, studies of the ryanodine receptor RyR1 [120–122] showed that apo CaM activated it, while calcium-saturated CaM inhibited it, showing that switching could be promoted by the addition or dissociation of calcium.

4.8 Power of Protein Ensembles

Prior to its recognition as a regulator of ion channels, studies of CaM revolved around its regulation of soluble enzymes including kinases, cyclases, phosphodiesterases, and phosphatases which are activated by $(Ca^{2+})_4$-CaM.[123–126] The two domains or lobes of CaM were viewed primarily as resulting from duplication of the gene for a primordial 4-helix bundle with metal-binding loops.[127–130] Having two sets of paired EF-hands could be an evolutionary advantage for increasing avidity for targets in signaling pathways and enlarging the recognition site, thereby amplifying the response to an influx of calcium from the external medium, or internal stores. As membrane-spanning receptors and channels came to be recognized as non-enzymatic targets of CaM, some of them, such as NMDA [79, 131, 132], RyR1 [133–135] and $Ca_V1.2$ [91], were found to bind apo CaM under resting conditions, but have a higher affinity for calcium-saturated CaM than apo CaM. In that respect, they were similar to kinases such as CaMKII.

Clearly, calcium-saturated CaM is a biologically significant state of CaM. In yeast, Davis and colleagues also demonstrated that apo CaM is essential to viability.[136–138] There are 16 states total: 14 possible intermediates with 1, 2 or 3 calcium ions bound. Structures of $(Ca^{2+})_{2-}$ CaM bound to a fragment of the SK channel (1G4Y), and the IQ motif region of $Na_V1.2$ (4JPZ) and $Na_V1.5$ (4JQ0) are examples of an intermediate partially ligated CaM. Half-saturated CaM has also been observed in reverse – with apo CaM_N and calcium-saturated CaM_C bound to the anthrax edema factor.[139] It is even possible that CaM with one or three calcium ions bound may also have a significant role in some physiological processes. CaBP1 (Calcium Binding Protein 1) binds only 3 Ca^{2+}, suggesting that there are some neuronal targets that prefer this stoichiometry.[140] Wild-type CaM with 4 functional sites is unlikely to adopt states with only one site filled in a domain because of the high degree of cooperativity between calcium-binding sites in the same domains. However, interactions between binding-site residues in CaM and side chains of residues in a target protein could alter the energetic balance to tip it in favor of an unoccupied site as proposed in the analysis of 4DCK.[22]

In neurons, sodium channels with multiple binding sites for auxiliary proteins integrate input from a panoply of modulators including CaM. In the structure reported here (2M5E), we showed that calcium saturation of CaM bound to the IQ motif of $Na_V1.2$ triggers a half-turn rotation of CaM_C around I_{1912} which has structural consequences for the geometry of CaM_N as well as CaM_C. The physiological consequences must be explored further. Having determined what CaM does on an isolated IQ motif, it remains to be seen whether CaM reverses polarity in solution on the full CTD of $Na_V1.2$, and how the binding of intracellular FGFs (FHFs) may influence CaM-IQ interactions. Just as regulatory pathways in genetic circuits quantitatively integrate the effects of multiple proteins binding to DNA, and interacting both directly and allosterically with each other[141], neurons can take advantage of the full ensemble of energetically accessible states for auxiliary proteins binding to channels, and make use of ligand-triggered changes in their flexible structures.

Supplementary Material

Refer to Web version on PubMed Central for supplementary material.

Acknowledgments

We thank A. Persechini and DJ Black for sharing a published vector used as the parent for the biosensor overexpression plasmid made in this study, and Sean A. Klein for critical input on experimental approaches.

These studies were supported by Iowa Center for Research by Undergraduates Fellowships to L.H., Z.L, and D.C.M,, a graduate fellowship for M.S.M. from the University of Iowa Center for Biocatalysis and Bioprocessing Training Grant in Biotechnology NIH T32 GM08365, a Biochemistry Summer Undergraduate Fellowship for B.C.W., the Roy J. Carver Charitable Trust Grant 01–224, and a grant to M.A.S. from the National Institutes of Health (R01 GM57001). The content is solely the responsibility of the authors and does not necessarily represent the official views of the National Institutes of Health.

Abbreviations

BAA	Basic, Amphipathic Alpha Helix
CaM	Calmodulin
CaMBD	Calmodulin-Binding Domain
CaMC	C-domain of CaM
CaM_N	N-domain of CaM
CFP	Cyan Fluorescent Protein
CTD	C-terminal Domain
EGTA	Ethylene Glycol Bis(aminoethylether)-N,N,N’,N’-tetra-acetic acid
FRET	Förster/Fluorescence Resonance Energy Transfer
HEPES	N-(2-hydroxy-ethyl)piperazine-N′-2-ethanesulfonic acid
HSQC	Heteronuclear Single Quantum Coherence
$Na_v1.2_{IQp}$	IQ motif peptide (residues 1901 to 1927) of rat $Na_V1.2$
Na_V	Voltage-gated Sodium Channel
NMR	Nuclear Magnetic Resonance
NOE	Nuclear Overhauser Effect
NTA	Nitrilo-triacetic acid
RMSD	Root-Mean-Squared Deviation
YFP	Yellow Fluorescent Protein

References

1. Catterall WA. From Ionic Currents to Molecular Mechanisms: The Structure and Function of Voltage-Gated Sodium Channels. Neuron. 2000; 26:13–25. [PubMed: 10798388]
2. Schaller KL, Caldwell JH. Expression and distribution of voltage-gated sodium channels in the cerebellum. Cerebellum. 2003; 2:2–9. [PubMed: 12882229]

3. Meisler MH, Kearney J, Ottman R, Escayg A. Identification of epilepsy genes in human and mouse. Annual Review of Genetics. 2001; 35:567–588.
4. Rook MB, Bezzina Alshinawi C, Groenewegen WA, van Gelder IC, van Ginneken AC, Jongsma HJ, Mannens MM, Wilde AA. Human SCN5A gene mutations alter cardiac sodium channel kinetics and are associated with the Brugada syndrome. Cardiovascular research. 1999; 44:507–517. [PubMed: 10690282]
5. Weiss LA, Escayg A, Kearney JA, Trudeau M, MacDonald BT, Mori M, Reichert J, Buxbaum JD, Meisler MH. Sodium channels SCN1A, SCN2A and SCN3A in familial autism. Molecular Psychiatry. 2003; 8:186–194. [PubMed: 12610651]
6. Meisler MH, Kearney JA. Sodium channel mutations in epilepsy and other neurological disorders. Journal of Clinical Investigation. 2005; 115:2010–2017. [PubMed: 16075041]
7. Kim J, Ghosh S, Liu H, Tateyama M, Kass RS, Pitt GS. Calmodulin mediates Ca^{2+} sensitivity of sodium channels. Journal of Biological Chemistry. 2004; 279:45004–45012. [PubMed: 15316014]
8. Cheung WY. Calmodulin Plays a Pivotal Role in Cellular Regulation. Science. 1980; 207:19–27. [PubMed: 6243188]
9. Ben-Johny M, Yang PS, Niu J, Yang W, Joshi-Mukherjee R, Yue DT. Conservation of Ca^{2+}/Calmodulin Regulation across Na and Ca^{2}+ Channels. Cell. 2014; 157:1657–1670. [PubMed: 24949975]
10. Yu FH, Catterall WA. Overview of the voltage-gated sodium channel family. Genome Biology. 2003; 4:207.201–207.207. [PubMed: 12620097]
11. Wildburger NC, Ali SR, Hsu WC, Shavkunov AS, Nenov MN, Lichti CF, LeDuc RD, Mostovenko E, Panova-Elektronova NI, Emmett MR, Nilsson CL, Laezza F. Quantitative proteomics reveals protein-protein interactions with fibroblast growth factor 12 as a component of the voltage-gated sodium channel 1.2 ($Na_V1.2$) macromolecular complex in Mammalian brain. Molecular and Cellular Proteomics. 2015; 14:1288–1300. [PubMed: 25724910]
12. Miloushev VZ, Levine JA, Arbing MA, Hunt JF, Pitt GS, Palmer AG. Solution structure of the $Na_V1.2$ C-terminal EF-hand domain. Journal of Biological Chemistry. 2009; 284:6446–6454. [PubMed: 19129176]
13. Rhoads AR, Friedberg F. Sequence motifs for calmodulin recognition. The Federation of American Societies for Experimental Biology Journal. 1997; 11:331–340. [PubMed: 9141499]
14. Mori M, Konno T, Ozawa T, Murata M, Imoto K, Nagayama K. Novel Interaction of the Voltage-Dependent Sodium Channel (VDSC) with Calmodulin: Does VDSC Acquire Calmodulin-Mediated Ca^{2+}-Sensitivity? Biochemistry. 2000; 39:1316–1323. [PubMed: 10684611]
15. Theoharis NT, Sorensen BR, Theisen-Toupal J, Shea MA. The Neuronal Voltage-Dependent Sodium Channel Type II IQ Motif Lowers the Calcium Affinity of the C-Domain of Calmodulin. Biochemistry. 2008; 47:112–123. [PubMed: 18067319]
16. Feldkamp MD, Yu L, Shea MA. Structural and Energetic Determinants of Apo Calmodulin Binding to the IQ Motif of the $Na_V1.2$ Voltage-Dependent Sodium Channel. Structure. 2011; 19:733–747. [PubMed: 21439835]
17. Cormier JW, Rivolta I, Tateyama M, Yang AS, Kass RS. Secondary Structure of the Human Cardiac Na^{+} Channel C Terminus. Journal of Biological Chemistry. 2002; 277:9233–9241. [PubMed: 11741959]
18. Mantegazza M, Yu FH, Catterall WA, Scheuer T. Role of the C-terminal domain in inactivation of brain and cardiac sodium channel. Proceedings of the National Academy of Sciences of the United States of America. 2001; 98:15348–15353. [PubMed: 11742069]
19. Houdusse A, Gaucher JF, Krementsova E, Mui S, Trybus KM, Cohen C. Crystal structure of apo-calmodulin bound to the first two IQ motifs of myosin V reveals essential recognition features. Proceedings of the National Academy of Sciences of the United States of America. 2006; 103:19326–19331. [PubMed: 17151196]
20. Schumacher MA, Rivard AF, Bachinger HP, Adelman JP. Structure of the gating domain of a Ca^{2+}-activated K+ channel complexed with Ca^{2+}/calmodulin. Nature. 2001; 410:1120–1124. [PubMed: 11323678]
21. Chagot B, Chazin WJ. Solution NMR Structure of Apo-Calmodulin in Complex with the IQ Motif of Human Cardiac Sodium Channel $Na_V1.5$. Journal of molecular biology. 2011; 406:106119.

22. Wang C, Chung BC, Yan H, Lee SY, Pitt GS. Crystal Structure of the Ternary Complex of a Na_V C-Terminal Domain, a Fibroblast Growth Factor Homologous Factor, and Calmodulin. Structure. 2012
23. Gabelli SB, Boto A, Kuhns VH, Bianchet MA, Farinelli F, Aripirala S, Yoder J, Jakoncic J, Tomaselli GF, Amzel LM. Regulation of the $Na_V1.5$ cytoplasmic domain by calmodulin. Nature communications. 2014; 5:5126.
24. Reddy Chichili VP, Xiao Y, Seetharaman J, Cummins TR, Sivaraman J. Structural basis for the modulation of the neuronal voltage-gated sodium channel $Na_V1.6$ by calmodulin. Scientific reports. 2013; 3:2435. [PubMed: 23942337]
25. Strynadka NCJ, James MNG. Crystal Structures of the Helix-Loop-Helix Calcium-Binding Proteins. Annual Review of Biochemistry. 1989; 58:951–998.
26. Crooks GE, Hon G, Chandonia JM, Brenner SE. WebLogo: a sequence logo generator. Genome Research. 2004; 14:1188–1190. [PubMed: 15173120]
27. Kim EY, Rumpf CH, Fujiwara Y, Cooley ES, Van Petegem F, Minor DL Jr. Structures of Ca_V2 Ca^{2+}/CaM-IQ domain complexes reveal binding modes that underlie calcium-dependent inactivation and facilitation. Structure. 2008; 16:1455–1467. [PubMed: 18940602]
28. Cantrell AR, Catterall WA. Neuromodulation of Na+ Channels: An Unexpected Form of Cellular Plasticity, Nature Reviews. Neuroscience. 2001; 2:397–407. [PubMed: 11389473]
29. Ikura M, Ames JB. Genetic polymorphism and protein conformational plasticity in the calmodulin superfamily: two ways to promote multifunctionality. Proceedings of the National Academy of Sciences of the United States of America. 2006; 103:1159–1164. [PubMed: 16432210]
30. Meador WE, Means AR, Quiocho FA. Modulation of calmodulin plasticity in molecular recognition on the basis of X-ray structures. Science. 1993; 262:1718–1721. [PubMed: 8259515]
31. Homouz D, Sanabria H, Waxham MN, Cheung MS. Modulation of calmodulin plasticity by the effect of macromolecular crowding. Journal of molecular biology. 2009; 391:933–943. [PubMed: 19577574]
32. Villarroel A, Taglialatela M, Bernardo-Seisdedos G, Alaimo A, Agirre J, Alberdi A, Gomis-Perez C, Soldovieri MV, Ambrosino P, Malo C, Areso P. The ever changing moods of calmodulin: how structural plasticity entails transductional adaptability. Journal of molecular biology. 2014; 426:2717–2735. [PubMed: 24857860]
33. Wang C, Chung BC, Yan H, Wang HG, Lee SY, Pitt GS. Structural analyses of Ca^{2+}/CaM interaction with Na_V channel C-termini reveal mechanisms of calcium-dependent regulation. Nature communications. 2014; 5:4896.
34. Chagot B, Potet F, Balser JR, Chazin WJ. Solution NMR structure of the C-terminal EF-hand domain of human cardiac sodium channel $Na_V1.5$, Journal of. Biological Chemistry. 2009; 284:6436–6445.
35. Feldkamp MD, Yu L, Shea MA. Calmodulin Regulation of the Neuronal Voltage-Dependent Sodium Channel. Biophysical journal. 2010; 98:310.
36. Strynadka NCJ, James MNG. Model for the Interaction of Amphiphilic Helices With Troponin C and Calmodulin, Proteins: Structure. Function, and Genetics. 1990; 7:234–248.
37. LaPorte DC, Wierman BM, Storm DR. Calcium-induced exposure of a hydrophobic surface on calmodulin. Biochemistry. 1980; 19:3814–3819. [PubMed: 6250577]
38. Black DJ, Leonard J, Persechini A. Biphasic Ca^{2+}-dependent switching in a calmodulin-IQ domain complex. Biochemistry. 2006; 45:6987–6995. [PubMed: 16734434]
39. Sarhan MF, Van Petegem F, Ahern CA. A double tyrosine motif in the cardiac sodium channel domain III-IV linker couples calcium-dependent calmodulin binding to inactivation gating. Journal of Biological Chemistry. 2009; 284:33265–33274. [PubMed: 19808664]
40. Sarhan MF, Tung CC, Van Petegem F, Ahern CA. Crystallographic basis for calcium regulation of sodium channels. Proceedings of the National Academy of Sciences of the United States of America. 2012; 109:3558–3563. [PubMed: 22331908]
41. Shah VN, Wingo TL, Weiss KL, Williams CK, Balser JR, Chazin WJ. Calcium-dependent regulation of the voltage-gated sodium channel hH1: intrinsic and extrinsic sensors use a common molecular switch. Proceedings of the National Academy of Sciences of the United States of America. 2006; 103:3592–3597. [PubMed: 16505387]

42. Lee A, Zhou H, Scheuer T, Catterall WA. Molecular determinants of Ca^{2+}/calmodulin-dependent regulation of $Ca_V2.1$ channels. Proceedings of the National Academy of Sciences of the United States of America. 2003; 100:16059–16064. [PubMed: 14673106]
43. Lee A, Scheuer T, Catterall WA. Ca^{2+}/calmodulin-dependent facilitation and inactivation of P/Q-type Ca^{2+} channels. Journal of Neuroscience. 2000; 20:6830–6838. [PubMed: 10995827]
44. Dick IE, Tadross MR, Liang H, Tay LH, Yang W, Yue DT. A modular switch for spatial Ca^{2+} selectivity in the calmodulin regulation of Ca_V channels. Nature. 2008; 451:830–834. [PubMed: 18235447]
45. Zhou H, Yu K, McCoy KL, Lee A. Molecular mechanism for divergent regulation of $Ca_V1.2$ Ca^{2+} channels by calmodulin and Ca^{2+}-binding protein-1. Journal of Biological Chemistry. 2005; 280:29612–29619. [PubMed: 15980432]
46. Leal K, Mochida S, Scheuer T, Catterall WA. Fine-tuning synaptic plasticity by modulation of $Ca_V2.1$ channels with Ca^{2+} sensor proteins. Proceedings of the National Academy of Sciences of the United States of America. 2012; 109:17069–17074. [PubMed: 23027954]
47. Putkey JA, Slaughter GR, Means AR. Bacterial expression and characterization of proteins derived from the chicken calmodulin cDNA and a calmodulin processed gene. Journal of Biological Chemistry. 1985; 260:4704–4712. [PubMed: 2985564]
48. Smith PK, Krohn RI, Hermanson GT, Mallia AK, Gartner FH, Provenzano MD, Fujimoto EK, Goeke NM, Olson BJ, Klenk DC. Measurement of Protein Using Bicinchoninic Acid. Analytical Biochemistry. 1985; 150:76–85. [PubMed: 3843705]
49. Beaven GH, Holiday ER. Ultraviolet absorption spectra of proteins and amino acids. Advances in Protein Chemistry. 1952; 7:319–386. [PubMed: 14933256]
50. Romoser VA, Hinkle PM, Persechini A. Detection in living cells of Ca^{2+}-dependent changes in the fluorescence emission of an indicator composed of two green fluorescent protein variants linked by a calmodulin-binding sequence. A new class of fluorescent indicators. Journal of Biological Chemistry. 1997; 272:13270–13274. [PubMed: 9148946]
51. Tsien RY. The green fluorescent protein. Annual Review of Biochemistry. 1998; 67:509544.
52. Johnson ML, Frasier SG. Nonlinear Least-Squares Analysis. Methods in Enzymology. 1985; 117:301–342.
53. Sorensen BR, Shea MA. Interactions between domains of apo calmodulin alter calcium binding and stability. Biochemistry. 1998; 37:4244–4253. [PubMed: 9521747]
54. VanScyoc WS, Newman RA, Sorensen BR, Shea MA. Calcium Binding by Calmodulin Mutants Having Domain-Specific Effects on Regulation of Ion Channels. Biochemistry. 2006; 45:14311–14324. [PubMed: 17128970]
55. Delaglio F, Grzesiek S, Vuister GW, Zhu G, Pfeifer J, Bax A. NMRPipe: a multidimensional spectral processing system based on UNIX pipes. Journal of Biomolecular NMR. 1995; 6:277–293. [PubMed: 8520220]
56. Goddard TD, Kneller DG. SPARKY, University of California, San Francisco.
57. Vranken WF, Boucher W, Stevens TJ, Fogh RH, Pajon A, Llinas M, Ulrich EL, Markley JL, Ionides J, Laue ED. The CCPN data model for NMR spectroscopy: development of a software pipeline. Proteins. 2005; 59:687–696. [PubMed: 15815974]
58. Bahrami A, Assadi AH, Markley JL, Eghbalnia HR. Probabilistic interaction network of evidence algorithm and its application to complete labeling of peak lists from protein NMR spectroscopy. PLoS computational biology. 2009; 5:e1000307. [PubMed: 19282963]
59. Gemmecker G, Olejniczak ET, Fesik SW. An Improved Method for Selectively Observing Protons Attached to C-12 in the Presence of H-1-C-13 Spin Pairs. Journal of magnetic resonance. 1992; 96:199–204.
60. Ikura M, Bax A. Isotope-Filtered 2D NMR of a Protein-Peptide Complex: Study of a Skeletal Muscle Myosin Light Chain Kinase Fragment Bound to Calmodulin. Journal of the American Chemistry Society. 1992; 114:2433–2440.
61. Otting G, Wuthrich K. Extended Heteronuclear Editing of 2d H-1-Nmr Spectra of Isotope-Labeled Proteins, Using the X(Omega-1, Omega-2) Double Half Filter. Journal of magnetic resonance. 1989; 85:586–594.

62. Burgering MJ, Boelens R, Caffrey M, Breg JN, Kaptein R. Observation of inter-subunit nuclear Overhauser effects in a dimeric protein. Application to the Arc repressor, FEBS Letters. 1993; 330:105–109. [PubMed: 8370451]
63. Cheung MS, Maguire ML, Stevens TJ, Broadhurst RW. DANGLE: A Bayesian inferential method for predicting protein backbone dihedral angles and secondary structure. Journal of magnetic resonance. 2010; 202:223–233. [PubMed: 20015671]
64. Shen Y, Delaglio F, Cornilescu G, Bax A. TALOS+: a hybrid method for predicting protein backbone torsion angles from NMR chemical shifts. Journal of Biomolecular NMR. 2009; 44:213–223. [PubMed: 19548092]
65. Rieping W, Habeck M, Bardiaux B, Bernard A, Malliavin TE, Nilges M. ARIA2: automated NOE assignment and data integration in NMR structure calculation. Bioinformatics. 2007; 23:381–382. [PubMed: 17121777]
66. Brunger AT, Adams PD, Clore GM, DeLano WL, Gros P, Grosse-Kunstleve RW, Jiang JS, Kuszewski J, Nilges M, Pannu NS, Read RJ, Rice LM, Simonson T, Warren GL. Crystallography & NMR system: A new software suite for macromolecular structure determination. Acta Crystallographics Section D Biological Crystallography. 1998; 54:905–921. [PubMed: 9757107]
67. Schwieters CD, Kuszewski JJ, Tjandra N, Clore GM. The Xplor-NIH NMR molecular structure determination package. Journal of magnetic resonance. 2003; 160:65–73. [PubMed: 12565051]
68. Schwieters CD, Kuszewski JJ, Clore GM. Using Xplor-NIH for NMR molecular structure determination. Progress in nuclear magnetic resonance spectroscopy. 2006; 48:47–62.
69. Wilson MA, Brunger AT. The 1.0 A Crystal Structure of Ca^{2+}-bound Calmodulin: an Analysis of Disorder and Implications for Functionally Relevant Plasticity. Journal of Molecular Biology. 2000; 301:1237–1256. [PubMed: 10966818]
70. Laskowski RA, Rullmannn JA, MacArthur MW, Kaptein R, Thornton JM. AQUA and PROCHECK-NMR: programs for checking the quality of protein structures solved by NMR. Journal of Biomolecular NMR. 1996; 8:477–486. [PubMed: 9008363]
71. Newman RA, Van Scyoc WS, Sorensen BR, Jaren OR, Shea MA. Interdomain cooperativity of calmodulin to melittin preferentially increases calcium affinity of sites I and II. Proteins: Structure, Function, and Bioinformatics. 2008; 71:1792–1812.
72. Coulomb CA. Premier mémoire sur l'électricité et le magnétisme Histoire de l'Académie Royale des Sciences, (. 1785:569–577.
73. Sobolev V, Sorokine A, Prilusky J, Abola EE, Edelman M. Automated analysis of interatomic contacts in proteins. Bioinformatics. 1999; 15:327–332. [PubMed: 10320401]
74. Yamniuk AP, Vogel HJ. Calmodulin's flexibility allows for promiscuity in its interactions with target proteins and peptides. Molecular Biotechnology. 2004; 27:33–57. [PubMed: 15122046]
75. Ataman ZA, Gakhar L, Sorensen BR, Hell JW, Shea MA. The NMDA Receptor NR1 C1 Region Bound to Calmodulin: Structural Insights into Functional Differences between Homologous Domains. Structure. 2007; 15:1603–1617. [PubMed: 18073110]
76. Ishida H, Vogel HJ. Protein-peptide interaction studies demonstrate the versatility of calmodulin target protein binding. Protein and Peptide Letter. 2006; 13:455–465.
77. Peersen OB, Madsen TS, Falke JJ. Intermolecular tuning of calmodulin by target peptides and proteins: differential effects on Ca^{2+} binding and implications for kinase activation. Protein Science. 1997; 6:794–807. [PubMed: 9098889]
78. O'Donnell SE, Yu L, Fowler CA, Shea MA. Recognition of beta-calcineurin by the domains of calmodulin: thermodynamic and structural evidence for distinct roles. Proteins. 2011; 79:765–786. [PubMed: 21287611]
79. Akyol Z, Bartos JA, Merrill MA, Faga LA, Jaren OR, Shea MA, Hell JW. Apo–Calmodulin Binds with its COOH-terminal Domain to the N-methyl-D-aspartate Receptor NR1 C0 Region. Journal of Biological Chemistry. 2004; 279:2166–2175. [PubMed: 14530275]
80. Sonnenburg WK, Seger D, Kwak KS, Huang J, Charbonneau H, Beavo JA. Identification of inhibitory and calmodulin-binding domains of the PDE1A1 and PDE1A2 calmodulin-stimulated cyclic nucleotide phosphodiesterases. Journal of Biological Chemistry. 1995; 270:30989–31000. [PubMed: 8537356]

81. Black DJ, LaMartina D, Persechini A. The IQ domains in neuromodulin and PEP19 represent two major functional classes. Biochemistry. 2009; 48:11766–11772. [PubMed: 19877718]
82. Gerendasy DD, Herron SR, Jennings PA, Sutcliffe JG. Calmodulin stabilizes an amphiphilic a-helix within RC3/neurogranin and GAP-43/neuromodulin only when Ca^{2+} is absent. Journal of Biological Chemistry. 1995; 270:6741–6750. [PubMed: 7896819]
83. Liu Y, Storm DR. Regulation of free calmodulin levels by neuromodulin: Neuron growth and regeneration. TIPS. 1990; 11:107–111. [PubMed: 2151780]
84. Gerendasy DD, Herron SR, Watson JB, Sutcliffe JG. Mutational and biophysical studies suggest RC3/neurogranin regulates calmodulin availability. Journal of Biological Chemistry. 1994; 269:22420–22426. [PubMed: 8071370]
85. Martin SR, Bayley PM. Regulatory implications of a novel mode of interaction of calmodulin with a double IQ-motif target sequence from murine dilute myosin V. Protein Science. 2002; 11:2909–2923. [PubMed: 12441389]
86. Black DJ, Persechini A. Variations at the semiconserved glycine in the IQ domain consensus sequence have a major impact on Ca^{2+}-dependent switching in calmodulin-IQ domain complexes. Biochemistry. 2010; 49:78–83. [PubMed: 19954189]
87. Black DJ, Persechini A. In calmodulin-IQ domain complexes, the Ca^{2+}-free and Ca^{2+}-bound forms of the calmodulin l direct the N-lobe to different binding sites. Biochemistry. 2011; 50:10061–10068. [PubMed: 21999573]
88. Putkey JA, Kleerekoper Q, Gaertner TR, WAxham MN. A New Role for IQ Motif Proteins in Regulating Calmodulin Function. Journal of Biological Chemistry. 2003; 278:49667–49670. [PubMed: 14551202]
89. Evans TIA, Hell J, Shea MA. Thermodynamic Linkage Between Calmodulin Domains Binding Calcium and Contiguous Sites in the C-Terminal Tail of $Ca_V1.2$. Biophysical Chemistry. 2011; 159:172–187. [PubMed: 21757287]
90. Findeisen F, Tolia A, Arant R, Young Kim E, Isacoff E, Minor DL Jr. Calmodulin overexpression does not alter $Ca_V1.2$ function or oligomerization state. Channels. 2011; 5
91. Peterson BZ, DeMaria CD, Yue DT. Calmodulin Is the Ca^{2+} Sensor for Ca^{2+}-Dependent Inactivation of L-Type Calcium Channels. Neuron. 1999; 22:549–558. [PubMed: 10197534]
92. Ben-Johny M, Dick IE, Yue D, Yang W, Issa JB, Sang L, Lee SR, Limpitikul WB, Niu J, Kang PW, Banerjee R, Babich JS, Namkung H, Li J, Zhang M, Yang PS, Yue DN. Towards a Unified Theory of Calmodulin Regulation (Calmodulation) of Voltage-Gated Calcium and Sodium Channels. Current Molecular Pharmacology. 2014:1–18. [PubMed: 25713862]
93. Clapperton JA, Martin SR, Smerdon SJ, Gamblin SJ, Bayley PM. Structure of the Complex of Calmodulin with the Target Sequences of Calmodulin-Dependent Protein Kinase I: Studies of the Kinase Activation Mechanism. Biochemistry. 2002; 41:14669–14679. [PubMed: 12475216]
94. Tran QK, Black DJ, Persechini A. Dominant affectors in the calmodulin network shape the time courses of target responses in the cell. Cell Calcium. 2005; 37:541–553. [PubMed: 15862345]
95. Tran QK, Leonard J, Black DJ. A. Persechini, Phosphorylation within an autoinhibitory domain in endothelial nitric oxide synthase reduces the Ca^{2+} concentrations required for calmodulin to bind and activate the enzyme. Biochemistry. 2008; 47:7557–7566. [PubMed: 18558722]
96. Black DJ, Tran QK, Persechini A. Monitoring the total available calmodulin concentration in intact cells over the physiological range in free Ca^{2+} Cell Calcium. 2004; 35:415–425. [PubMed: 15003851]
97. Maier LS, Ziolo MT, Bossuyt J, Persechini A, Mestril R, Bers DM. Dynamic changes in free Ca-calmodulin levels in adult cardiac myocytes. Journal of Molecular and Cellular Cardiology. 2006; 41:451–458. [PubMed: 16765983]
98. Mori MX, Erickson MG, Yue DT. Functional Stoichiometry and Local Enrichment of Calmodulin Interacting with Ca^{2+} Channels. Science. 2004; 304:432–435. [PubMed: 15087548]
99. Li R, Leblanc J, He K, Liu XJ. Spindle function in Xenopus oocytes involves possible nanodomain calcium signaling. Molecular Biology of the Cell. 2016; 27:3273–3283. [PubMed: 27582389]
100. Bosch MK, Nerbonne JM, Townsend RR, Miyazaki H, Nukina N, Ornitz DM, Marionneau C. Proteomic analysis of native cerebellar iFGF14 complexes. Channels. 2016; 10:297–312. [PubMed: 26889602]

101. Young KA, Caldwell JH. Modulation of skeletal and cardiac voltage-gated sodium channels by calmodulin. Journal of Physiology. 2005; 565:349–370. [PubMed: 15746172]
102. Shen M, Zhang N, Zheng S, Zhang WB, Zhang HM, Lu Z, Su QP, Sun Y, Ye K, Li XD. Calmodulin in complex with the first IQ motif of myosin-5a functions as an intact calcium sensor. Proceedings of the National Academy of Sciences of the United States of America. 2016; 113:E5812–E5820. [PubMed: 27647889]
103. Chen LT, Liang WX, Chen S, Li RK, Tan JL, Xu PF, Luo LF, Wang L, Yu SH, Meng G, Li KK, Liu TX, Chen Z, Chen SJ. Functional and molecular features of the calmodulin-interacting protein IQCG required for haematopoiesis in zebrafish. Nature Communications. 5:3811.
104. Adsit GS, Vaidyanathan R, Galler CM, Kyle JW, Makielski JC. Channelopathies from mutations in the cardiac sodium channel protein complex. Journal of Molecular and Cellular Cardiology. 2013; 61:34–43. [PubMed: 23557754]
105. Chen Y, Clarke OB, Kim J, Stowe S, Kim YK, Assur Z, Cavalier M, Godoy-Ruiz R, von Alpen DC, Manzini C, Blaner WS, Frank J, Quadro L, Weber DJ, Shapiro L, Hendrickson WA, Mancia F. Structure of the STRA6 receptor for retinol uptake. Science. 2016; 353
106. Yus-Najera E, Santana-Castro I, Villarroel A. The identification and characterization of a noncontinuous calmodulin-binding site in noninactivating voltage-dependent KCNQ potassium channels. Journal of Biological Chemistry. 2002; 277:28545–28553. [PubMed: 12032157]
107. Ling KY, Preston RR, Burns R, Kink JA, Saimi Y, Kung C. Primary Mutations in Calmodulin Prevent Activation of the Ca^{2+}-Dependent Na^{+} Channel in Paramecium, Proteins: Structure. Function, and Genetics. 1992; 12:365–371.
108. Kung C, Preston RR, Maley ME, Ling KY, Kanabrocki JA, Seavey BR, Saimi Y. In vivo Paramecium mutants show that calmodulin orchestrates membrane responses to stimuli. Cell Calcium. 1992; 13:413–425. [PubMed: 1380404]
109. Schaefer WH, Hinrichsen RD, Burgess-Cassler A, Kung C, Blair IA, Watterson DM. A mutant Paramecium with a defective calcium-dependent potassium conductance has an altered calmodulin: A nonlethal selective alteration in calmodulin regulation. Proceedings of the National Academy of Sciences of the United States of America. 1987; 84:3931–3935. [PubMed: 2438688]
110. Hennessey TM, Kung C. An anticalmodulin Drug, W-7, inhibits the voltage-dependent calcium current in Paramecium caudatum. Journal of Experimental Biology. 1984; 110:169181.
111. Ohya Y, Botstein D. Structure-based systematic isolation of conditional-lethal mutations in the single yeast calmodulin gene. Genetics. 1994; 138:1041–1054. [PubMed: 7896089]
112. Makita N, Yagihara N, Crotti L, Johnson CN, Beckmann BM, Roh MS, Shigemizu D, Lichtner P, Ishikawa T, Aiba T, Homfray T, Behr ER, Klug D, Denjoy I, Mastantuono E, Theisen D, Tsunoda T, Satake W, Toda T, Nakagawa H, Tsuji Y, Tsuchiya T, Yamamoto H, Miyamoto Y, Endo N, Kimura A, Ozaki K, Motomura H, Suda K, Tanaka T, Schwartz PJ, Meitinger T, Kaab S, Guicheney P, Shimizu W, Bhuiyan ZA, Watanabe H, Chazin WJ, George AL. Novel Calmodulin (CALM2) Mutations Associated with Congenital Arrhythmia Susceptibility. Circulation: Cardiovascular Genetics. 2014
113. Limpitikul WB, Dick IE, Joshi-Mukherjee R, Overgaard MT, George AL Jr, Yue DT. Calmodulin mutations associated with long QT syndrome prevent inactivation of cardiac L-type Ca currents and promote proarrhythmic behavior in ventricular myocytes. Journal Molecular and Cellular Cardiology. 2014
114. Crotti L, Johnson CN, Graf E, De Ferrari GM, Cuneo BF, Ovadia M, Papagiannis J, Feldkamp MD, Rathi SG, Kunic JD, Pedrazzini M, Wieland T, Lichtner P, Beckmann BM, Clark T, Shaffer C, Benson DW, Kaab S, Meitinger T, Strom TM, Chazin WJ, Schwartz PJ, George AL Jr. Calmodulin mutations associated with recurrent cardiac arrest in infants. Circulation. 2013; 127:1009–1017. [PubMed: 23388215]
115. Sondergaard MT, Sorensen AB, Skov LL, Kjaer-Sorensen K, Bauer MC, Nyegaard M, Linse S, Oxvig C, Overgaard MT. Calmodulin mutations causing catecholaminergic polymorphic ventricular tachycardia confer opposing functional and biophysical molecular changes. FEBS Journal. 2015; 282:803–816. [PubMed: 25557436]
116. Saimi Y, Kung C. Ion Channel regulation by calmodulin binding. FEBS Letter. 1994; 350:155–158.

117. Saimi Y, Kung C. Calmodulin as an Ion-Channel Subunit. Annual Review of Physiology. 2002; 64:289–311.
118. Ehlers MD, Augustine GJ. Cell signalling. Calmodulin at the channel gate, Nature, 399 (. 1999; 105:107–108.
119. van Petegem F, Chatelain FC, Minor DL Jr. Insights into voltage-gated calcium channel regulation from the structure of the $Ca_{(V)}1.2$ IQ domain-Ca^{2+}/calmodulin complex. Nature Structural and Molecular Biology. 2005; 12:1108–1115.
120. Hamilton SL. Ryanodine Receptors. Cell Calcium. 2005; 38:253–260. [PubMed: 16115682]
121. Xiong LW, Newman RA, Rodney GG, Thomas O, Zhang JZ, Persechini A, Shea MA, Hamilton SL. Lobe-dependent regulation of ryanodine receptor type 1 by calmodulin. Journal of Biological Chemistry. 2002; 277:40862–40870. [PubMed: 12185083]
122. Yamaguchi N, Xin C, Meissner G. Identification of apocalmodulin and Ca^{2+}-calmodulin regulatory domain in skeletal muscle Ca^{2+} release channel, ryanodine receptor. Journal of Biological Chemistry. 2001; 276:22579–22585. [PubMed: 11306590]
123. Crivici A, Ikura M. Molecular and Structural Basis of Target Recognition by Calmodulin. Annual Review of Biophysics and Biomolecular Structure. 1995; 24:85–116.
124. Klee, CB. Interaction of calmodulin with Ca^{2+} and target proteins. In: Cohen, P., Klee, CB., editors. Calmodulin. Elsevier; New York: 1988. p. 35-56.
125. Klee CB, Vanaman TC. Calmodulin, Advances in Protein Chemistry. 1982; 35:213321.
126. Klee CB, Ren H, Wang X. Regulation of the calmodulin-stimulated protein phosphatase, calcineurin. Journal of Biological Chemistry. 1998; 273:13367–13370. [PubMed: 9593662]
127. Gifford JL, Walsh MP, Vogel HJ. Structures and metal-ion-binding properties of the Ca^{2+}-binding helix-loop-helix EF-hand motifs. Biochemical Journal. 2007; 405:199–221. [PubMed: 17590154]
128. Kretsinger RH. Structure and Evolution of Calcium-Modulated Proteins. Critical Review in Biochemistry and Molecular Biology. 1980; 8:119–174.
129. Persechini A, Moncrief ND, Kretsinger RH. The EF-hand family of calcium-modulated proteins. Trends in Neurosciences. 1989; 12(11):462–467. [PubMed: 2479149]
130. McPhalen CA, Strynadka NCJ, James MNG. Calcium-Binding Sites in Proteins: A Structural Perspective. Advances in Protein Chemistry. 1991; 42:77–144. [PubMed: 1793008]
131. Ehlers MD, Zhang S, Bernhardt JP, Huganir RL. Inactivation of NMDA receptors by direct interaction of calmodulin with the NR1 subunit. Cell. 1996; 84:745–755. [PubMed: 8625412]
132. Zhang S, Ehlers MD, Bernhardt JP, Su CT, Huganir RL. Calmodulin mediates calcium-dependent inactivation of N-methyl-D-aspartate receptors. Neuron. 1998; 21:443–453. [PubMed: 9728925]
133. Moore CP, Rodney G, Zhang JZ, Santacruz-Toloza L, Strasburg G, Hamilton SL. Apocalmodulin and Ca^{2+} calmodulin bind to the same region on the skeletal muscle Ca^{2+} release channel. Biochemistry. 1999; 38:8532–8537. [PubMed: 10387100]
134. Rodney GG, Williams BY, Strasburg GM, Beckingham K, Hamilton SL. Regulation of RYR1 Activity by Ca^{2+} and Calmodulin. Biochemistry. 2000; 39:7807–7812. [PubMed: 10869186]
135. Samsó M, Wagenknecht T, Allen PD. Internal structure and visualization of transmembrane domains of the RyR1 calcium release channel by cryo-EM. Nature Structural & Molecular Biology. 2005; 12:539–544.
136. Geiser JR, van Tuinen D, Brockerhoff SE, Neff MM, Davis TN. Can Calmodulin Function without Binding Calcium? Cell. 1991; 65:949–959. [PubMed: 2044154]
137. Davis TN, Thorner J. Vertebrate and yeast calmodulin, despite significant sequence divergence, are functionally interchangeable. Proceedings of the National Academy of Sciences of the United States of America. 1989; 86:7909–7913. [PubMed: 2554295]
138. Davis TN, Urdea MS, Masiarz FR, Thorner J. Isolation of the Yeast Calmodulin Gene: Calmodulin Is an Essential Protein. Cell. 1986; 47:423–431. [PubMed: 3533275]
139. Drum CL, Yan S, Bard J, Shen Y, LU D, Soelaiman S, Grabarek Z, Bohm A, Tang W. Structural basis for the activation of anthrax adenylyl cyclase exotoxin by calmodulin. Nature. 2002; 415:396–402. [PubMed: 11807546]

140. Park S, Li C, Ames JB. Nuclear magnetic resonance structure of calcium-binding protein 1 in a Ca^{2+}-bound closed state: implications for target recognition. Protein Science. 2011; 20:1356–1366. [PubMed: 21608059]

141. Shea MA, Ackers GK. The O_R Control System of Bacteriophage Lambda A physical-chemical model for gene regulation. Journal of Molecular Biology. 1985; 181:211–230. [PubMed: 3157005]

142. Shea MA, Miller MS, Yoder JB, Fowler CA, Feldkamp MD, Yu L. Calcium-Mediated Tailspin of Calmodulin on the IQ Motif of the Neuronal Voltage-Dependent Sodium Channel $Na_V1.2$. Biophysical Journal. 2013; 104:14a.

143. Miller MS, Fowler CA, Feldkamp MD, Yu L, Shea MA. Calcium-Mediated Reversal of CaM on the $Na_V1.2$ IQ Motif: Nested Anti-Parallel Sites. Biophysical Journal. 2014; 106:48a.

Highlights

1. $Na_V1.2$ IQ motif binds apo and $(Ca^{2+})_4$-CaM tightly: how can Ca^{2+} binding trigger change?
2. Direct measure of equilibrium Kd values: apo CaM (~3 nM) vs. $(Ca^{2+})_4$-CaM (~85 nM).
3. Solution structure of $(Ca^{2+})_2$-CaM_C bound to $Na_V1.2$ IQ has “open” EF-hand conformation.
4. 2KXW and 2M5E are first NMR structures of apo and Ca^{2+}-CaM_C bound to same channel.
5. CaM binds nested, anti-parallel sites in $Na_V1.2$ IQ; Ca^{2+} binding to CaM_C reverses its orientation.

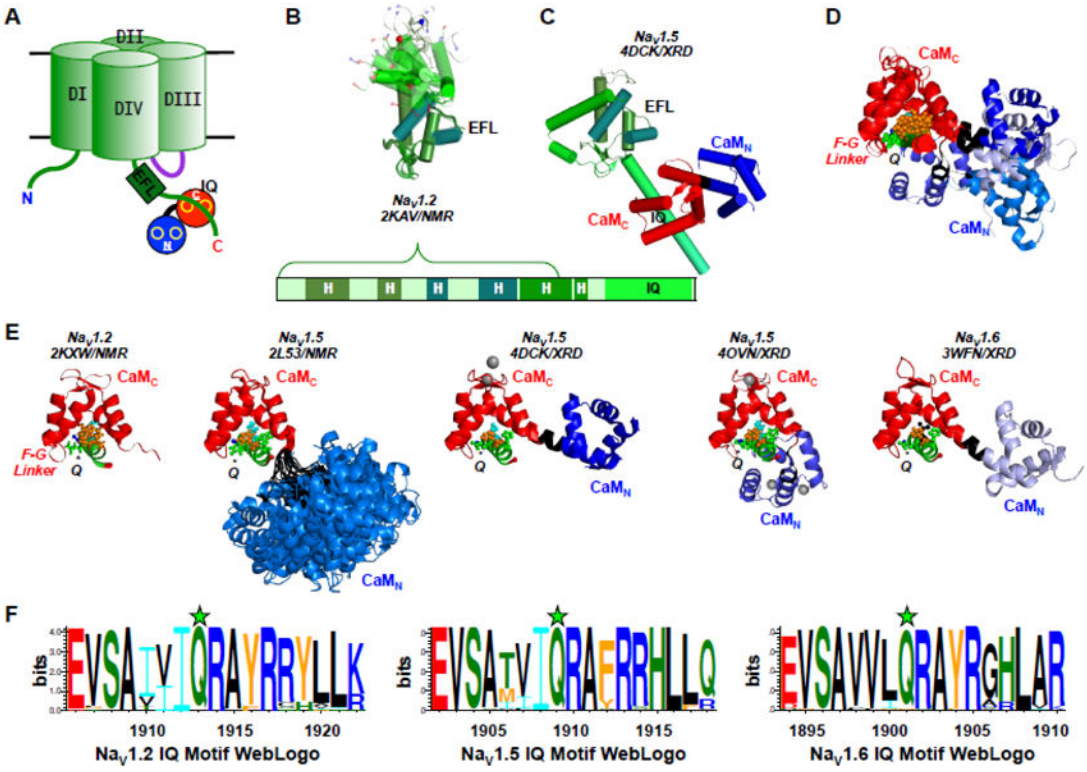

Figure 1. Schematics and Structures of CaM Binding to Na_V IQ Motifs

In all structures of CaM, residues 1–75 are blue, 76–80 are black, and 81–148 are red.

A: Cartoon of a voltage-gated sodium channel (Na_V) α-subunit (green) with 4 multi-helical transmembrane units DI, DII, DIII, and DIV (cylinders). The C-terminal domain (CTD) contains a 4-helix bundle domain dubbed EF-like (EFL) and an lQ motif bound to apo CaM_C (red) with apo CaM_N (blue) connected by a flexible linker (black). The Na_V inactivation gate (purple) links DIII and DIV, and contains a site for binding $(Ca^{2+})_4$-CaM.

B: Solution structures of the $Na_V1.2$ EF-like domain (PDB: 2KAV) depicting residues E1777 (blue sphere) to R1881 (red sphere); cylindrical helices are colored in shades of green correspond to the sections labeled H in the linear diagram of the $Na_V1.2$ CTD residues 1777 to 1937 below.

C: Crystallographic structure of apo (calcium-depleted) CaM bound to a CTD fragment of $Na_V1.5$ (PDB: 4DCK); shades of green match panel B. The $Na_V1.2$ CTD in 4DCK was aligned (using PyMOL (Schrödinger, LLC)) to the corresponding residues in 2KAV in panel B based on EFL-located helical residues 1791–1866 and 1855–1866.

D: Overlay of structures having apo or Mg^{2+}-bound CaM associated with Na_V IQ motifs (PDB: 2KXW, 2L53, 4DCK, 4OVN, and 3WFN). For structures determined by NMR (2KXW and 2L53), only the minimized average structure is shown. Structures aligned with PyMOL (Schrödinger, LLC) based on position of CaM residues 102–112 and 117–128 (helices F and G).

E: Structures of individual CaM-IQ complexes in overlay in panel D; Mg^{2+} ions are gray spheres. For 2L53, all deposited models consistent with the NMR data are illustrated. Structures were aligned as in panel D. Spheres highlight IQ motif residues at positions 1, 2,

5 and 8. In, Nav1.2IQp these are I_{1912} (cyan), Q_{1913} (green), Y_{1916} and Y_{1919} (gold). In $Nav1.5_{IQp}$ and $Na_v1.6_{IQp}$, colors for corresponding residues match WebLogos in panel F. **F:** WebLogo 3.3[26] analyses comparing IQ motif sequences for $Na_V1.2$ from 53 species, $Na_V1.5$ from 40 species and $Na_V1.6$. from 45 species (sequence alignments shown in Supplemental Tables S1A, S1B, S1C). The height of each letter denotes relative conservation of residues. A star indicates the fully conserved Q residue of all three channels which is also labeled in panel E. Within the set of residues binding apo CaM_C, complete conservation is observed for positions corresponding to Q_{1913}, R_{1914}, A_{1915}, R_{1917} in $Na_V1.2$.

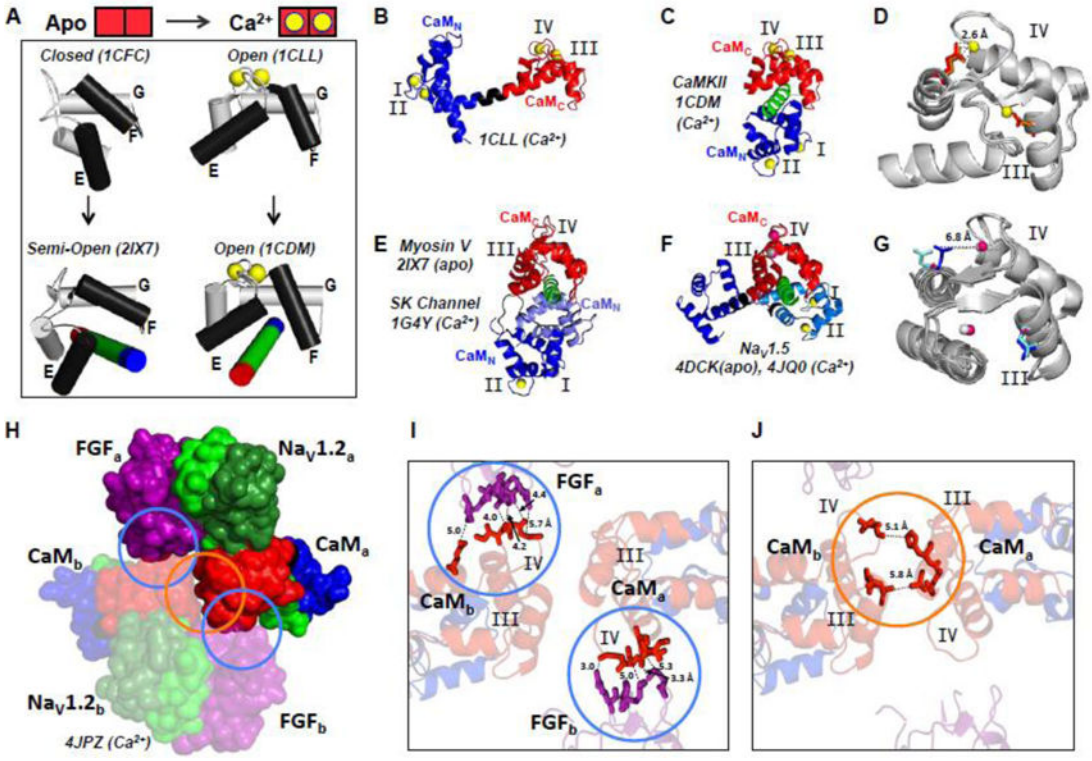

Figure 2. Ca^{2+}-Induced Changes in Calmodulin Structure and Linkage to Target Binding

A. Schematic showing structural changes of CaM_C upon binding Ca^{2+} (horizontal) and a peptide target (vertical). Structures were aligned by CaM residues 117–128 (helix G). Interhelical angles for helices E and F (http://calcium.sci.yokohama-cu.ac.jp/efhand.html) shown in black are as follows: apo CaM_C (1CFC, 54.8°), apo CaM_C bound to an IQ motif in myosin V (2IX7, 79.5°), $(Ca^{2+})_2$-CaM_C (1CLL, 89.7°), and $(Ca^{2+})_2$-CaM_C bound to CaMKII (1CDM, 88.5°). For 2IX7 and 1CDM, the termini of the green target peptide are blue (amino) and red (carboxyl).

B. $(Ca^{2+})_4$-CaM in 1CLL. CaM residues 1–75 are blue, 76–80 are black, and 81–148 are red; Ca^{2+} ions are yellow.

C. $(Ca^{2+})_4$-CaM bound to CaMKII peptide in 1CDM. Color scheme the same as panel B, with peptide in green.

D. Alignment of CaM_C residues in B and C showing E104 and E140 in 1CLL (orange) and 1CDM (red) as sticks in Ca^{2+}-binding sites. Label gives the average distance between carboxyl oxygens of E140 and the Ca^{2+} in site IV. CaM_C in each structure is shown in gray; structures were aligned using CaM residues 102–112 and 117–128 (helices F and G).

E. Overlay of apo CaM bound to a myosin V IQ motif in 2IX7, and half-saturated CaM (CaM_N Ca^{2+}-saturated but CaM_C apo) bound to an SK Channel peptide (1G4Y) aligned by CaM_C helices F and G.

F. Apo (Mg^{2+}-bound) CaM and $(Ca^{2+})_4$-CaM bound to $Na_V1.5$ IQ motif (4DCK and 4JQ0). In sites III and IV, Mg^{2+} is gray, and Ca^{2+} ions listed in 4JQ0 are hot pink. Structures were aligned as in panel A.

G. Alignment of apo CaM_C bound to SK Channel (1G4Y) shown in panel E, and apo (Mg^{2+} bound CaM_C) bound to $Na_V1.5$ (4DCK) and $(Ca^{2+})_4$-CaM bound to $Na_V1.5$ IQ motif

(4JQ0) shown in panel F. Side chains of E104 and E140 in 1G4Y (cyan) and 4DCK (blue) are shown as sticks; only backbone atoms for E104 and E140 were assigned in 4JQ0 (hot pink). Label gives the average distance between carboxyl oxygens of E140 and the Mg^{2+} ion in site IV in 4DCK. Mg^{2+} is gray, and Ca^{2+} assigned in 4JQ0 is hot pink.

H. Dimer of heterotrimers (Na_V-FGF13U-CaM) in the 4JPZ crystal structure of $(Ca^{2+})_4$-CaM bound to $Na_V1.2$ CTD (residues 1777–1937, green) and FGF13U (purple). Circled regions correspond to regions circled in panels I and J.

I. Blue circles highlight multiple contacts (≤ 6Å) between CaM in one heterotrimer of 4JPZ with FGF13U in the other heterotrimer. Heterotrimers are labeled with subscripts “a” and “b” for tracking interactions. They are identical in sequence, and nearly identical structurally.

J. Orange circle highlights highlight contacts (≤ 6Å) between CaM_C in one heterotrimer of 4JPZ with CaM_C in the other.

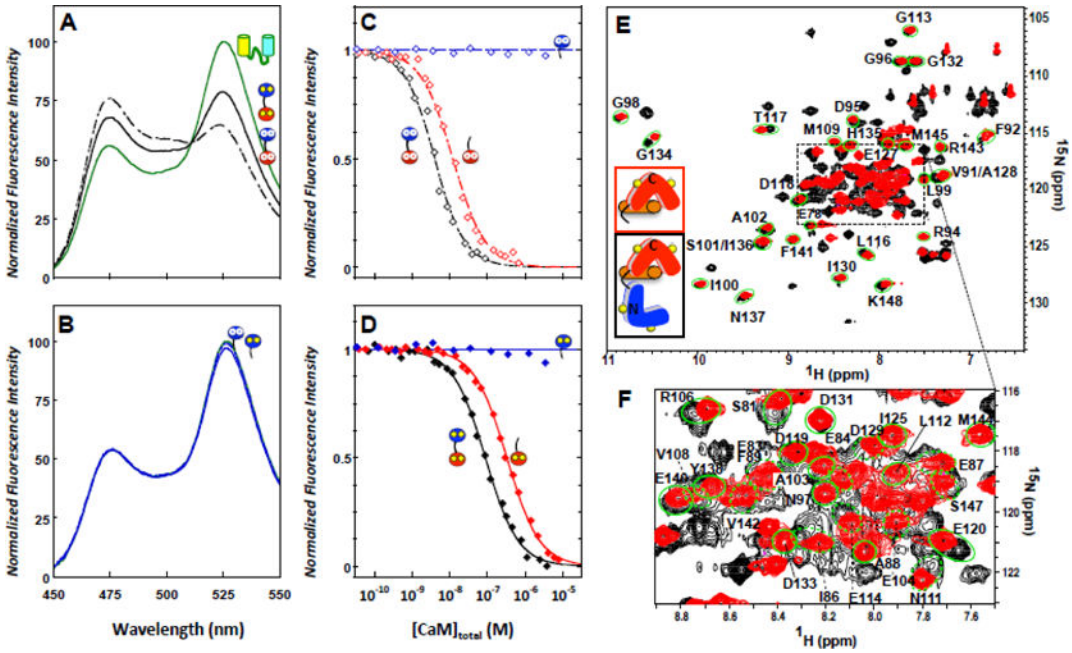

Figure 3. CaM Binding to $Na_V1.2IQ$ Biosensor and $Na_V1.2$ IQp

$Na_v1.2_{IQ}$ biosensor samples excited at 430 nm; peaks in emission intensity correspond to CFP (475 nm) and YFP (525 nm).

A. Steady-state emission spectra of $Na_v1.2_{IQ}$ biosensor alone (solid green) and saturated with apo CaM (black dashed) or calcium-saturated CaM (black solid) (>10^3-fold excess).

B. Emission spectra of $Na_v1.2_{IQ}$ biosensor alone (solid green) and with >10^3-fold excess apo CaMN (blue solid) and calcium-saturated CaMN (blue dashed).

C. Equilibrium titrations of biosensor binding by apo full-length CaM (black dashed), CaMC (red dashed), and CaM_N (blue dashed).

D. Equilibrium titrations of biosensor binding by calcium-saturated full-length CaM (black solid), CaMC (red solid), and CaMN (blue solid). Simulations in panels C and D are based on fits to the experimental data set shown in each panel. For CaMN, a horizontal line is provided to guide the eye.

E. ^{15}N-HSQC spectral overlay of $(Ca^{2+})_2$-CaM_C (red) and $(Ca^{2+})_4$-CaM (black) bound to $Na_v1.2_{IQp}$ (black). Backbone resonance assignments are shown for residues of peptide-bound CaM_C. Green ellipses encircle resonances for the same residue in each complex.

F. Expansion of crowded region of spectral overlay in panel E.

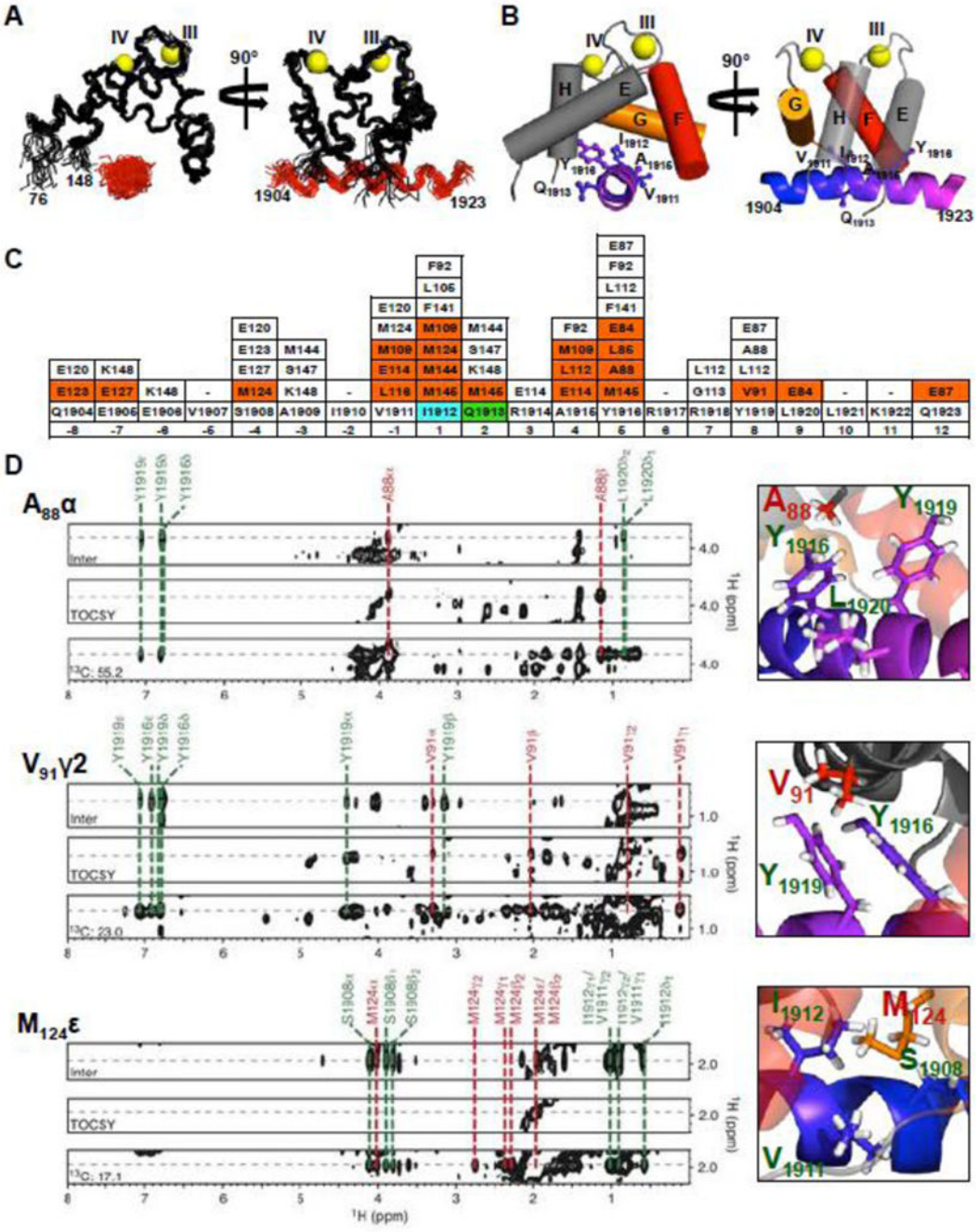

Figure 4. NMR Models of Ca^{2+}-Saturated CaM_C Bound to $Na_V1.2_{IQp}$

A. Wireframe backbone representations of the 20 lowest energy structures and the ensemble minimized average model of $(Ca^{2+})_2$-CaM_C bound to $Na_v1.2_{IQp}$ (2M5E). For clarity, only well ordered helical residues 1904–1923 of $Na_v1.2_{IQp}$ are shown.

B. Cartoon representation of minimized average model in 2M5E. $Na_v1.2_{IQp}$ helix shown as a ribbon with gradient from blue (N-terminus) to magenta (C-terminus). Cylinders represent CaM helices E (gray), F (red), G (orange) and H (gray) with yellow spheres for calcium ions. Residues of the IQ motif making ≥ 3 short-range contacts (< 4.5 Å) with the

hydrophobic cleft of CaM are shown in ball-and-stick representation along with Q_{1913} for reference.

C. Analysis by CSU (Contacts of Structural Units)[73] of the minimized average model of $(Ca^{2+})_2$-CaM_C-$Na_v1.2_{IQp}$. The primary sequence of residues 1904 to 1923 of the IQ motif is shown on the x-axis (I_{1912} in cyan, Q_{1913} in green). Boxes listing residues of CaM located within 4.5 Å of each IQ motif residue are shaded in orange; longer range contacts (4.5 to 6 Å) are in white boxes.

D. NMR strip plots corresponding to three CaM residues: A88α, V91γ2 and M124ε. For each residue, the top panel represents a ^{13}C-edited, ^{12}C,^{14}N-filtered NOESY experiment, the middle panel represents an HCCH-TOCSY experiment, and the bottom panel is a ^{13}C-edited NOESY with carbon chemical shift of the planes denoted in the label. Labels for atoms in $Na_v1.2_{IQp}$ are green and in CaM are red. Residues surrounding A_{83}, V_{91} and M_{124} of CaM are shown in images made with PyMOL (Schrödinger, LLC) next to the strip plots.

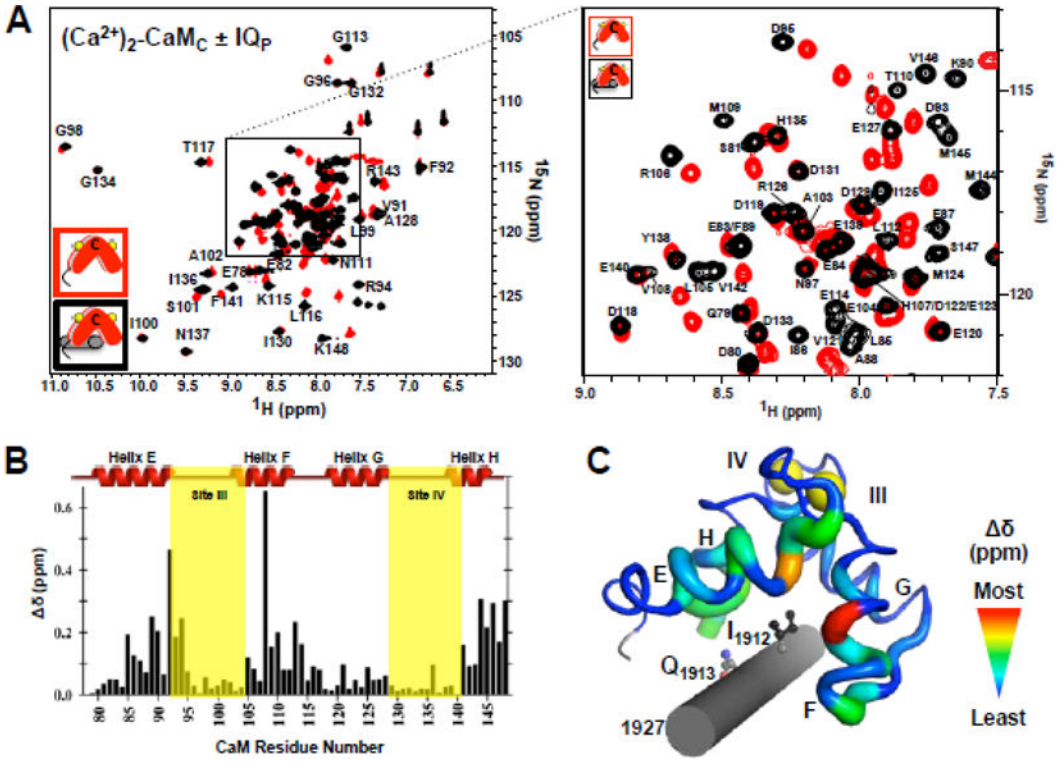

Figure 5. Chemical Shift Differences and Contacts in $(Ca^{2+})_2$-CaM_C ± $Na_v1.2|_{Qp}$

A. HSQC spectral overlay of $(Ca^{2+})_2$-CaM_C alone (red) and bound to $Na_v1.2_{IQp}$ (black). Backbone resonance assignments are shown for residues of peptide-bound CaM_C.

B. Effects of $Na_v1.2_{IQp}$ on chemical shifts of $(Ca^{2+})_2$-CaM_C. Changes in chemical shifts are calculated as described in Methods. Location of CaM helices and calcium-binding loops are shown above the plot. Residues in calcium-binding sites III (93–104) and IV (128–140) are indicated by yellow shading.

C. Chemical shift perturbations mapped onto the structure of $(Ca^{2+})_2$-CaMC in 2M5E. The greatest effect of $Na_v1.2_{IQp}$ binding is indicated by the red/wide cartoon, and the weakest effect is shown by the blue/narrow cartoon.

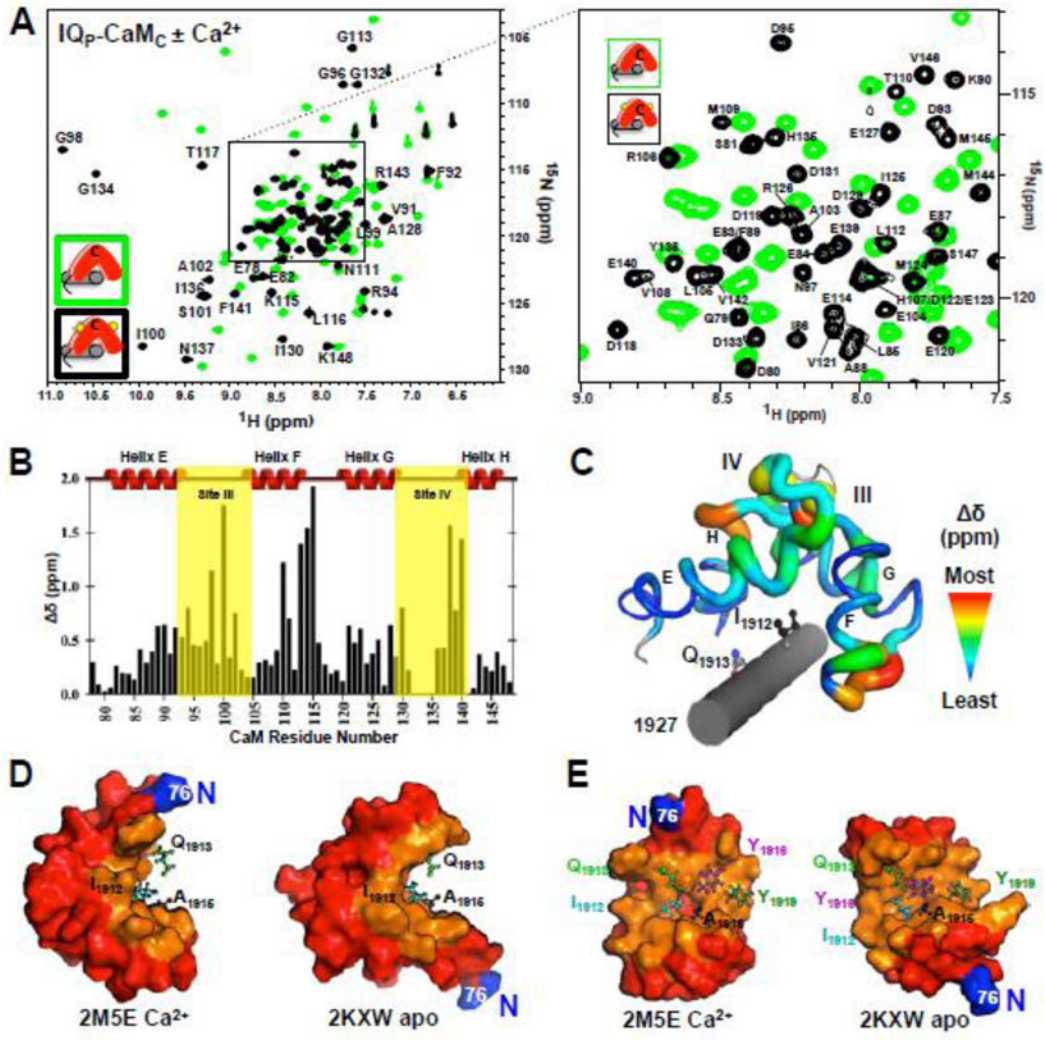

Figure 6. Comparison of Nested Anti-Parallel Sites in $Na_V1.2_{IQp}$

A. HSQC overlay of CaM_C-$Na_V1.2_{IQp}$ with (black) and without (green) saturating calcium. Backbone resonance assignments are shown for residues of $(Ca^{2+})_2$-CaM-$Na_V1.2_{IQp}$.

B. Chemical shift differences between CaM_C-$Na_V1.2_{IQp}$ ± Ca^{2+} indicated changes in chemical environment of individual CaM residues. Location of CaM helices and calcium-binding loops are shown above the plot. Residues in calcium-binding sites III (93–104) and IV (128–140) are indicated by yellow shading.

C. Chemical shift perturbations mapped onto the structure of $(Ca^{2+})_2$-CaM_C in 2M5E. The greatest effect of Ca^{2+} binding is shown in the cartoon as red/wide, while the weakest effect is blue/narrow.

D. Comparison of $(Ca^{2+})_2$-CaM_C (2M5E) and apo CaM_C (2KXW) bound to $Na_V1.2_{IQp}$ aligned by superposition of the helical backbone of $Na_V1.2_{IQp}$. Residues I_{1912} (cyan), Q_{1913} (green), and A_{1915} (black) are in ball-and-stick. For clarity, the peptide backbone is omitted. The surface of solvent-exposed CaM residues is red and cleft residues are orange in semi-open (2KXW) and open (2M5E) CaM. CaM_N would connect to CaM_C via residue M76 (blue) highlighting the reversed orientations of CaM_C on the IQ motif.

E. Comparison of clefts of Ca^{2+}-CaM_C (2M5E) and apo CaM_C (2KXW) binding $Na_v1.2_{IQp}$. Structures were aligned based on helical residues of the peptide. IQ motif residues I_{1912} (cyan) Q_{1913} (green), A_{1915} (black), Y_{1916} (magenta), and Y_{1919} (dark green) are shown in ball-and-stick representation. For clarity, the backbone of the peptide is not shown.

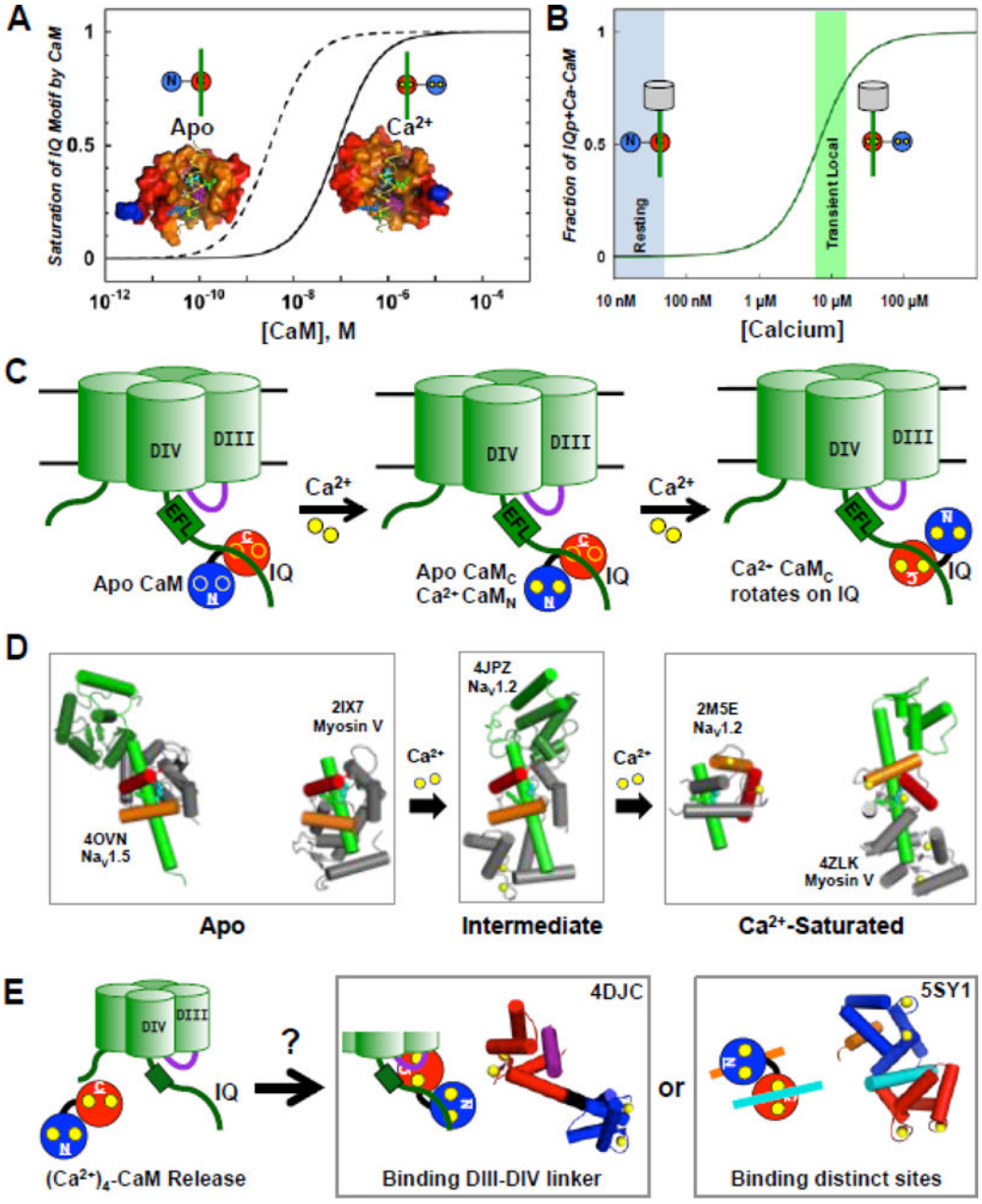

Figure 7. Models of CaM Retention, Release, or Reversal on $Na_V1.2$

A. Simulations of saturation of the $Na_V1.2$ IQ motif by apo (dashed) and calcium-saturated (solid) CaM based on ΔG values in Table 1. Molecular models show calcium-induced reversal of CaM_C relative to the IQ motif peptide.

B. Simulation of calcium binding to CaM bound to the $Na_V1.2$ IQ motif (see *Methods).* Resting calcium levels indicated by blue bar; green bar centered on 10 03BCM indicates range of neuronal intracellular Ca^{2+} levels sufficient to achieve 50–75% calcium-saturated CaM_C bound to $Na_V1.2$-IQ. Schematics indicate calcium-induced reversal of CaM_C on the IQ motif.

C. Schematic for proposed 3-state mechanism of CaM-mediated regulation based on calcium titration of full-length CaM bound to $Na_V1.2_{IQp}$ monitored by NMR. Apo CaM binds to the IQ motif via CaM_C with no preferred contacts between CaM_N and $Na_v1.2_{IQp}$. Calcium binding to sites I and II affects only CaM_N; calcium binding to sites III and IV triggers reversal of CaM_C on the IQ motif.

D. CaM-target structures representative of the 3 states shown schematically in part C. Target is green with spheres for the I (cyan) and Q (green) residues of the IQ motif. CaM is gray except for CaM_C helices F (red) and G (orange). Apo CaM bound to the $Na_V1.5$ IQ motif (4OVN) or an IQ motif of myosin V (2IX7) shows I oriented into the semi-open cleft, and Q oriented towards the FG-linker in semi-open CaM_C. The intermediate state of CaM bound to the $Na_V1.2$ IQ motif (4JPZ) retains the same orientation of CaM_C as the apo state. Ca^{2+}-saturated CaM adopts an open conformation bound to the IQ motif of $Na_V1.2$ (2M5E) and myosin V (4ZLK) with Q oriented towards the junction between CaM_N and CaM_C. All 5 structures were aligned by residues corresponding to 1909–1915 of $Na_V1.2$ in 2M5E, where Iis 1912 and Q is at 1913.

E. Alternative models of calcium-mediated response include $(Ca^{2+})_4$-CaM dissociation from $Na_V1.2$, which might promote $(Ca^{2+})_4$-CaM binding at the DIII–DIV linker (“inactivation gate”, purple) as seen in 4DJC, or binding at a pair of CaMBD sequences (orange, cyan) that are not in a continuous helix, such as seen in 5SY1, the STRA6 receptor for retinol uptake.

Table 1

Free Energy of CaM Binding to rNa$_V$1.2 IQ Motif

	Apo CaM			Calcium-Saturated CaM			
IQ	**ΔG_{Apo}** *1*	**K_d** *2*	**$\Delta\Delta G$** *3*	**$\Delta G_{Ca^{2+}}$**	**K_d**	**$\Delta\Delta G$** *3*	**$\Delta\Delta G$** *4* **Ca^{2+}—Apo**
CaM	−11.48 ± 0.18	3.2 nM		−9.55 ± 0.08	85 nM		+ 1.93
CaM_C	−10.72 ± 0.10	11.6 nM	+0.76	−8.66 ± 0.09	386 nM	+0.89	+2.06
CaM_N		>100 μM			>100 μM		

1 Values of ΔG reported in kcal/mol. Averages based on 4 to 7 determinations from at least 2 independent preparations of biosensors, and two independent preparations of CaM. Standard deviations from the mean are reported. Confidence intervals on independent trials ranged from ±.04 to ±.24 kcal/mol, with a median value of 0.10 kcal/mol.

2 K_d (equilibrium dissociation constant) calculated from average value of ΔG reported here.

3 $\Delta\Delta G = \Delta G_{CaMc} - \Delta G_{CaM}$

4 $\Delta\Delta G_{Ca2+-Apo} = \Delta G Ca^{2+} - \Delta G_{Apo}$

Solution Conditions: 50 mM HEPES, 100 mM KCl, 50 μM EGTA, 5 mM NTA, 1 mM $MgCl_2$, 1.5 μM BSA, 500 μM DTT, ± 1 mM $CaCl_2$; pH 7.4, 22 °C

Table 2

Structural Statistics for 2M5E* for the final ensemble (20 lowest energy structures)

Experimental restraints		
CaM NOEs[a]		
Intraresidue (i = j)	492	
Sequential (|i-j| =1)	393	
Medium range (1 < |i-j| < 5)	415	
Long range (|i-j| ≥ 5)	399	
Total CaM NOEs	1699	
Peptide NOEs	279	
Intermolecular NOEs	97	
Total unambiguous NOEs	2075	
NOEs with multiple assignments	651	
Total NOEs	2726	
Distance restraints per residue, CaM[a]	23.6	
Distance restraints per residue, peptide[b]	13.3	
phi/psi angles, CaM	136	
phi/psi angles, peptide	38	
Restraint violations	**ensemble**	**minimized average**
NOE distances violated > 0.2 Å	0	0
dihedral angles violated > 2°	0	0
RMSDs from experimental restraints		
NOE (Å)	0.0039 ± 0.0001	0.004
Dihedrals (°)	0.068 ± 0.021	0.082
XPLOR energies (kcal/mol)		
overall energy	50.63 ± 1.33	54.93
bonds	0.74 ± 0.06	1.00
angles	41.10 ± 0.28	41.92
impropers	1.02 ± 0.08	1.09
van der Waals	5.50 ± 0.96	8.67
NOEs	2.21 ± 0.12	2.17
dihedrals	0.05 ± 0.03	0.07
RMSD from idealized geometry		
Bond lengths (Å)	0.0007 ± 0.0001	0.0008
Bond angles (°)	0.300 ± 0.001	0.303
Impropers (°)	0.090 ± 0.003	0.093
Ramachandran plot statistics (%)[c]		
Most favored regions	92.0	90.6
Additionally allowed regions	7.6	9.4
Generously allowed regions	0.4	0.0
Disallowed regions	0.1	0.0

Experimental restraints

Coordinate RMSD (average difference to mean, Å)[c]	
Backbone atoms	0.643
Heavy atoms	1.188

Restraint violations, RMSDs and energies are for all residues in the construct. Structural statistics are taken from the output of CNS[66], with the exception of the Ramachandran statistics which come from PROCHECK-NMR. [70]

[a] for CaM residues 77–148 (all except M76)

[b] for peptide residues 1904–1924 (all assigned)

[c] for structured residues (CaM residues 79–147, peptide residues 1904–1924).